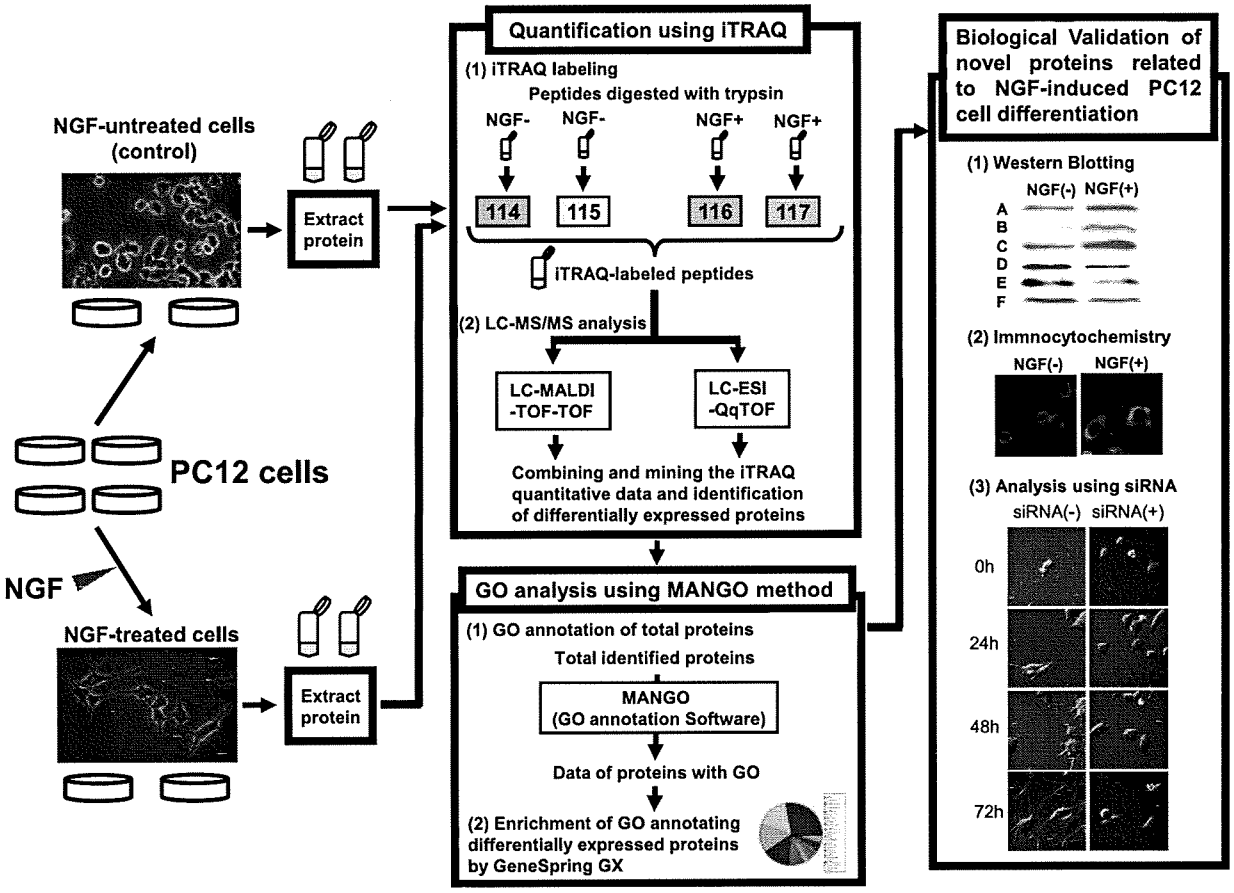

FIG. 1. **Work flow for the identification of the novel proteins regulating NGF-induced differentiation in PC12 cells.** For the fourplex iTRAQ labeling, the four lysates of PC12 cells separately cultured were prepared in parallel. The tryptic peptides from untreated cells and NGF-treated cells were labeled using mass 114/115 and 116/117 isobaric iTRAQ tags, respectively. These labeled peptides were analyzed with LC-MALDI-TOF-TOF or LC-ESI-QqTOF, and the quantification of each protein was performed according to the obtained iTRAQ data. Further biological and functional interpretation of the differentially expressed proteins was carried out by proteomics GO analysis using the MANGO method followed by cell biological analyses. Proteins *A–F* are candidates for novel molecules related to NGF-induced PC12 cell differentiation.

iTRAQ Sample Labeling—One hundred micrograms of each protein sample was precipitated using a 2-D Clean-Up kit (Amersham Biosciences), and the precipitants were dissolved in 10 μl of 6 M urea. iTRAQ sample labeling was performed according to the manufacturer's protocol with minimum modification. For the fourplex iTRAQ labeling, the four lysates of PC12 cells separately cultured were treated with iTRAQ reagents in parallel. Twenty microliters of dissolution buffer and 1 μl of denaturant reagent were added to the samples. The samples were reduced by addition of 2 μl of reducing reagent and incubation at 60 °C for 1 h. Reduced cysteine residues were then blocked by addition of 1 μl of cysteine blocking reagent and incubated at room temperature for a further 10 min. Tryptic digestion was initiated by the addition of 12.5 μl of trypsin solution (Promega; prepared as 1 μg/μl in water solution) and incubated at 37 °C for 16 h. To label the peptides with iTRAQ reagents, one vial of labeling reagent was thawed and reconstituted in 80 μl of ethanol. The reagents 114 and 115 for two samples from untreated cells and the reagents 116 and 117 for two samples from NGF-stimulated cells were added to the digests and incubated for 1 h at room temperature. The labeled samples were then mixed together before fractionation using a cation exchange column.

Sample Fractionation and Desalting—To remove excess, unbound iTRAQ reagent and to simplify the peptide mixture, the labeled peptide mixture was purified and fractionated using a GE Healthcare AKTA system. The mixed sample was diluted in loading buffer (20% (v/v) ACN and 10 mM potassium phosphate, pH 3.0) and loaded onto a Mono S column (GE Healthcare) equilibrated with loading buffer. Peptides were eluted with a gradient of solvent B (10 mM potassium phosphate, pH 3.0, and 1 M KCl in 20% (v/v) ACN) as follows: 0–2 min, 0–7% B; at 6 min, to 14% B; at 8 min, to 32% B; at 13 min, to 70% B; and at 21 min, to 100% B. Twenty-five fractions that included the iTRAQ-labeled peptides were used for analysis. The fractions were dried in a vacuum centrifuge and rehydrated with solution containing 2% ACN and 0.1% TFA. The samples were desalted with ZipTip™ μ-C_{18} pipette tips (Millipore). The desalted peptides were divided into two fractions to analyze the same samples by using nano-LC-MALDI-TOF-TOF and nano-LC-ESI-QqTOF systems.

LC-MALDI-MS/MS Analysis—Samples were separated by C_{18} nano-LC using DiNa Map (KYA Tech Corp.) equipped with a device spotting eluted fractions on a MALDI plate. Sample was injected onto a C_{18} column (0.5-mm inner diameter × 1-mm length, KYA Tech Corp.) equilibrated with solvent A (2% ACN and 0.1% TFA) and resolved on a C_{18} nanocolumn (0.15-mm inner diameter × 100-mm length; KYA Tech Corp.) at a flow rate of 300 nl/min with a 90-min gradient of solvent B (70% ACN and 0.1% TFA) as follows: 0–20% B from 0 to 10 min, to 50% B at 65 min, and to 100% B at 75 min. Column effluent was mixed with matrix (2 mg/ml α-cyano-4-hydroxycinnamic acid in 50% ACN and 0.1% TFA) at a flow rate of 1.4 μl/min.

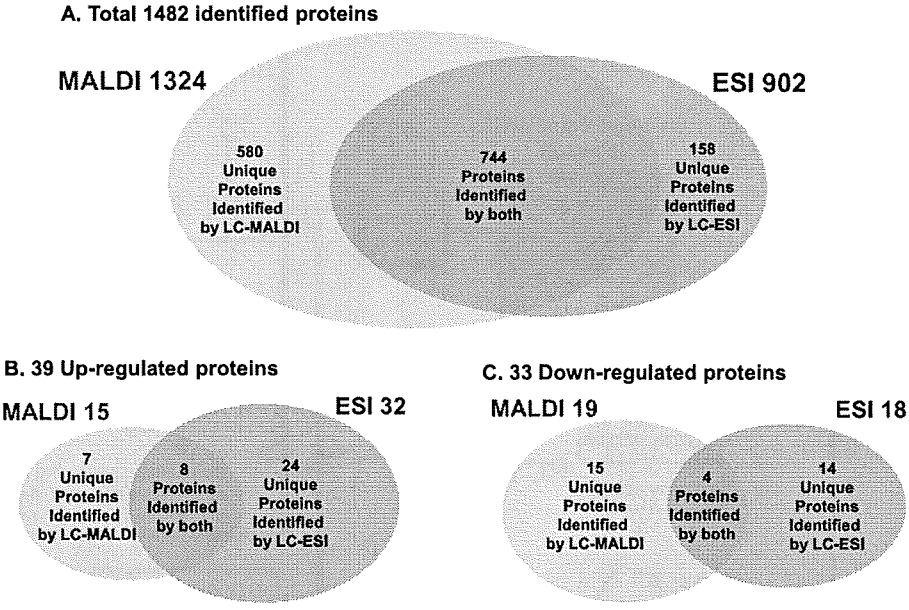

FIG. 2. **Venn diagrams of the number of total (*A*), up-regulated (*B*), and down-regulated (*C*) proteins identified by iTRAQ.** *A*, in total, 1,482 proteins of all taxonomies listed in supplemental Table 1 were identified with a confidence limit of 95%. *B* and *C*, for quantification of each protein identified by MALDI or ESI, a -fold change of each protein expression was calculated by comparing the average iTRAQ ratio of 116 and 117 as NGF-treated groups with the average ratio of 114 and 115 as control groups. Proteins quantified with a -fold change more than 20% (average iTRAQ ratio >1.20 or <0.83) and a *p* value less than 0.05 by MALDI or ESI were identified as differentially expressed proteins (*B* and *C*).

Fractions were spotted at 30-s intervals onto a stainless steel MALDI target plate (192 wells/plate; Applied Biosystems). Mass spectra of the peptides were acquired on a 4700 Proteomics Analyzer (Applied Biosystems) using 4000 Series Explorer software (Version 3.6). Mass spectra from *m/z* 800 to 4,000 were acquired for each fraction with 1,500 laser shots. To analyze the less abundant peptides, all of the peaks with a signal to noise ratio threshold from 50 to 75 and from 75 to 100 in each MS spectrum were selected for MS/MS analysis with 5,000 and 4,000 laser shots, respectively. Next all of the peaks above a signal to noise ratio threshold of 100 were selected for MS/MS analysis with 3,000 laser shots. Fragmentation of the labeled peptides was induced by the use of atmosphere as a collision gas with a pressure of 1×10^{-6} Torr and a collision energy of 1 kV.

LC-ESI-MS/MS Analysis—Samples were analyzed by nano-LC-ESI-MS/MS using the LC Packings Ultimate instrument fitted with a 20-μl sample loop. Samples were loaded onto a 5-mm RP C_{18} precolumn (LC Packings) at 30 μl/min and washed for 10 min before switching the precolumn in line with the separation column. The separation column used was a 75-μm internal diameter $\times$ 150-mm length PepMap RP column from LC Packings packed with 3-μm C_{18} beads with 100-Å pores. The flow rate used for separation on the RP column was 200 nl/min with a 90-min gradient of solvent B (85% ACN and 0.1% formic acid) as follows: 0–40% B from 0–60 min to 100% B at 70 min. The samples were divided into two fractions beforehand, and the first analysis was performed on a QSTAR Pulsar i mass spectrometer (Applied Biosystems/MDS Sciex), and the software used for data acquisition was Analyst QS 1.1 (Applied Biosystems/MDS Sciex) with the scan cycles set up to perform a 1-s MS scan followed by three MS/MS scans of the three most abundant peaks for 3 s each. Data acquisition was performed with an exclusion of 60 s for previous target ions. To analyze the less abundant peptides, the second analysis was performed under the same condition except for input of the *m/z* list to exclude the analyses of peptide ions already analyzed in the first run. The labeled peptides were fragmented under CID conditions designed to give iTRAQ reporter ions.

Data Analysis—Data from MALDI or ESI analysis were analyzed using the Paragon™ algorithm (30) of ProteinPilot Version 2.0 (Applied Biosystems), and the database searched was the Swiss-Prot database with all taxonomy (Revision number 53, 269,293 sequence entries, updated on May 29, 2007). Identified proteins were grouped by the Paragon algorithm of the software to minimize redundancy. This software has a function of automatic grouping of identified proteins according to the identified peptide sequence. The identified proteins were automatically grouping by the Paragon algorithm. Peptides used for the quantification of proteins were chosen by this algorithm of ProteinPilot software. All peptides used for the calculation of protein ratios were unique to the given protein or proteins within the group; peptides that were common to other isoforms or proteins of the same family that were reported separately were ignored. The ProteinPilot cutoff score used was 1.3, which corresponds to a confidence limit of 95%. The six user-defined options used included (i) cysteine alkylation, methyl methane thiosulfate; (ii) digestion, trypsin digestion; (iii) special factors, none; (iv) species, all species; (v) identification focus, biological modifications; and (vi) search effort, thorough identification search. For quantification of each protein identified in the MALDI or ESI analysis, a -fold change of each protein expression was calculated by comparing the average iTRAQ ratio of 116 and 117 as NGF-treated groups with the average ratio of 114 and 115 as control groups. Proteins quantified with a -fold change of more than 20% (average iTRAQ ratio >1.20 or <0.83) and a *p* value less than 0.05 (Student's *t* test) in the MALDI or ESI analysis were identified as differentially expressed proteins.

Proteomics GO Analysis by MANGO Method—To automate both the conversion of all identified proteins of multiple taxonomies into their human orthologs and annotation with GO information, a tool for taxonomy conversion/GO annotation, Molecular Annotation by Gene Ontology (MANGO), was designed as a Web-based application using the mySQL 4.0 database management system and scripts written in Java. Ensembl Mart and UniProt GOA (GOA UniProt Version 49.0, June 2007 update) files were integrated into the database and were used as the external reference data for the taxonomy conversion and the GO annotation, respectively. For the proteins that could not be automatically converted to the human orthologs using this conversion/annotation tool, we searched the human orthologs by using National Center for Biotechnology Information basic local alignment search tool (NCBI BLAST) programs. A list of 1,404 human GO-annotated proteins was compiled and was designated as the PC12 proteome reference set for analysis with GeneSpring GX (supplemental Table 4). GeneSpring GX Version 7.3.1 was used to determine the GO categories that were statistically overrepresented in the iTRAQ data set. GO categories, by which at least three proteins were annotated, were accepted at the significance level of $p < 0.05$ (Fisher's

TABLE I

List of proteins differentially-expressed in response to NGF stimulation

snRNA, small nuclear RNA; —, not applicable.

Protein name abbreviation	Protein name	Accession no.	Theoretical molecular mass (kDa)/pI	MALDI		ESI		Ref.[b]
				Average ratio[a]	*p* value	Average ratio[a]	*p* value	
Up-regulated proteins								
VGF	Neurosecretory protein VGF	P20156	68.2/4.7	**2.935**	0.011	**3.770**	0.024	23, 40
NEUM	Neuromodulin	P07936	23.6/4.6	**1.791**	0.008	**2.936**	0.021	23, 41
MOES	Moesin	O35763	67.7/6.2	**1.691**	0.035	**1.679**	0.030	—
CMGA	Chromogranin A	P10354	52.0/4.7	**1.594**	0.003	**1.596**	0.003	42
ANXA2	Annexin A2	Q07936	38.7/7.6	**1.449**	0.048	**1.805**	0.037	23, 43
PERI	Peripherin	P21807	53.5/5.4	**1.329**	0.011	**1.429**	0.012	44
AT1A1	Sodium/potassium-transporting ATPase α-1 chain	P06685	11.3/5.3	**1.271**	0.048	**1.341**	0.003	23
MAP1B	Microtubule-associated protein 1B	P15205	269.5/4.7	**1.250**	0.010	**1.352**	0.027	45
SQSTM	Sequestosome-1	O08623	47.7/5.1	**1.764**	0.042			—
RIR2	Ribonucleoside-diphosphate reductase M2 subunit	Q4KLN6	45.0/5.5	**1.339**	0.044			—
SGTA	Small glutamine-rich tetratricopeptide repeat-containing protein A	O70593	34.2/5.1	**1.286**	0.035	1.051	0.787	—
CROP	Cisplatin resistance-associated overexpressed protein	O95232[c]	51.5/9.8	**1.266**	0.042	1.006	0.294	—
PAIRBP1	Plasminogen activator inhibitor 1 RNA-binding protein	Q6AXS5	44.8/8.6	**1.226**	0.013	1.241	0.113	—
GSPT1	G_1 to S phase transition protein 1 homolog	P15170[c]	55.8/5.5	**1.206**	0.042	0.977	0.841	—
CRIP2	Cysteine-rich protein 2	P36201	22.7/8.9	**1.205**	0.020			—
PROTA	Prothymosin α	P06302	12.4/3.8	1.642	0.206	**2.173**	0.037	—
AHNAK	Neuroblast differentiation-associated protein AHNAK	Q09666[c]	629.1/5.8	1.245	0.113	**1.947**	0.012	46
SCG2	Secretogranin-2	P10362	71.0/4.7	1.339	0.068	**1.633**	0.027	42
AT1B1	Sodium/potassium-transporting ATPase subunit β-1	P07340	35.2/8.8	1.423	0.062	**1.630**	0.001	23
MAGED1	Melanoma-associated antigen D1	Q9ES73	85.8/7.1	1.066	0.654	**1.630**	0.020	—
LEG1	Galectin-1	P11762	14.9/5.1	1.272	0.126	**1.578**	0.016	22, 23
ENPL	Endoplasmin	P14625[c]	92.5/4.8	1.052	0.134	**1.556**	0.016	22, 23
S100A6	Protein S100-A6	P05964	10.0/5.3	1.362	0.069	**1.552**	0.004	—
E2IG5	E2-induced gene 5 protein homolog	Q4QQV3	17.8/10.0	1.240	0.103	**1.547**	0.023	23
CRMP4	Dihydropyrimidinase-related protein 3 (CRMP4)	Q62952	62.0/6.0	1.183	0.240	**1.407**	0.016	23
SRRM2	Serine/arginine repetitive matrix protein 2	Q8BTI8[d]	294.7/12.0	0.981	0.667	**1.377**	0.013	—
DNJA1	DnaJ homolog subfamily A member 1	P63036	44.9/6.7	1.065	0.397	**1.331**	0.011	—
RAC1	Ras-related C3 botulinum toxin substrate 1	Q6RUV5	21.5/8.8			**1.316**	0.044	—
TCTP	Translationally controlled tumor protein	P63029	19.5/4.8	1.359	0.126	**1.291**	0.016	—
RAB2A	Ras-related protein Rab-2A	P05712	23.5/6.1	1.272	0.239	**1.280**	0.015	—
OXRP	Hypoxia up-regulated protein 1	Q63617	111.3/5.1	1.051	0.591	**1.271**	0.008	—
PRDX6	Peroxiredoxin-6	O35244	24.8/5.6	1.128	0.207	**1.268**	0.008	—
ENOA	α-Enolase	P04764	47.1/6.2	1.153	0.172	**1.253**	0.008	23
RADI	Radixin	P35241[c]	68.6/6.0	0.885	0.193	**1.251**	0.032	23
ALDR	Aldose reductase	P07943	35.8/6.3	1.276	0.235	**1.248**	0.004	—
PDI	Protein-disulfide isomerase	P04785	57.0/4.8	1.041	0.118	**1.245**	0.045	23
FABPE	Fatty acid-binding protein, epidermal	P55053	15.1/6.73	1.136	0.268	**1.227**	0.049	23
RGP1	Ran GTPase-activating protein 1	P46061[d]	63.6/4.6	1.027	0.359	**1.219**	0.012	—
NUCB1	Nucleobindin-1	Q63083	53.5/5.0	1.039	0.521	**1.208**	0.005	—
Down-regulated proteins								
K1C18	Keratin, type I cytoskeletal 18	Q5BJY9	47.8/5.2	**0.626**	0.028	**0.566**	0.043	—
K2C8	Keratin, type II cytoskeletal 8	Q10758	54.0/5.8	**0.690**	0.011	**0.599**	0.040	—
PRPS2	Ribose-phosphate pyrophosphokinase II	P09330	34.8/6.2	**0.690**	0.040	**0.642**	0.015	—
LDHA	L-Lactate dehydrogenase A chain	P04642	36.5/8.5	**0.768**	0.022	**0.792**	0.041	—
PRP19	Pre-mRNA-processing factor 19	Q9JMJ4	55.2/6.2	**0.551**	0.009	0.880	0.604	—
VTDB	Vitamin D-binding protein	P04276	53.5/5.7	**0.625**	0.006			—
IDHP	Isocitrate dehydrogenase (NADP), mitochondrial	P56574	51.0/8.9	**0.630**	0.005	0.868	0.068	—
HNRLL	Heterogeneous nuclear ribonucleoprotein L-like	Q921F4[d]	64.1/5.8	**0.651**	0.031	0.636	0.187	—
NUCKS	Nuclear ubiquitous casein and cyclin-dependent kinase substrate	Q9EPJ0	27.1/5.0	**0.747**	0.006			—
API5	Apoptosis inhibitor 5	Q9BZZ5[c]	57.6/5.8	**0.748**	0.013	0.777	0.116	—
H2B1C	Histone H2B type 1	Q00715	14.0/10.4	**0.762**	0.040	0.860	0.003	23
RL34	60 S ribosomal protein L34	P11250	13.5/11.7	**0.769**	0.049			—
RLA0	60 S acidic ribosomal protein P0	P19945	34.2/5.9	**0.772**	0.035	0.962	0.605	—
TBB4	Tubulin β-4 chain	P04350[c]	49.6/4.8	**0.784**	0.034			—
SRR35	35-kDa SR repressor protein	Q8WXF0[c]	30.5/11.7	**0.787**	0.001			—
PCNA	Proliferating cell nuclear antigen	P04961	28.7/4.6	**0.790**	0.043	0.743	0.060	—

TABLE I—*continued*

Protein name abbreviation	Protein name	Accession no.	Theoretical molecular mass (kDa)/pI	MALDI		ESI		Ref.[b]
				Average ratio[a]	*p* value	Average ratio[a]	*p* value	
UBP48	Ubiquitin carboxyl-terminal hydrolase 48	Q76LT8	118.8/5.9	**0.793**	0.016			—
GSTM2	Glutathione *S*-transferase Mu 2	P08010	25.7/6.9	**0.794**	0.024	0.825	0.055	23
CB39L	Calcium-binding protein 39-like	Q9H9S4[c]	39.1/8.5	**0.818**	0.033			—
LSM8	U6 snRNA-associated Sm-like protein LSm8	O95777[c]	10.4/4.4			**0.648**	0.015	—
DDC	Aromatic-L-amino-acid decarboxylase	P14173	54.1/6.5			**0.669**	0.045	23
CSK21	Casein kinase II subunit α	P19139	45.1/7.3	0.875	0.088	**0.670**	0.041	—
RL6	60 S ribosomal protein L6	P21533	33.6/10.7	0.904	0.497	**0.681**	0.040	—
GALK1	Galactokinase	Q9R0N0[d]	42.2/5.2	1.222	0.509	**0.730**	0.029	—
AB14B	Abhydrolase domain-containing protein 14B	Q8VCR7[d]	22.5/5.8	0.675	0.292	**0.748**	0.030	—
HNRPF	Heterogeneous nuclear ribonucleoprotein F	Q794E4	45.7/5.3	1.053	0.294	**0.756**	0.031	—
APT	Adenine phosphoribosyltransferase	P36972	19.5/6.2	0.942	0.724	**0.783**	0.028	—
H2A2B	Histone H2A type 2-B	Q8IUE6[c]	14.0/10.9	0.860	0.157	**0.814**	0.024	23
FUBP2	Far upstream element-binding protein 2	Q99PF5	74.2/6.4	0.949	0.090	**0.818**	0.002	—
FINC	Fibronectin	P04937	272.5/5.5	0.688	0.172	**0.819**	0.000	—
TIM13	Mitochondrial import inner membrane translocase subunit Tim13	P62076	10.5/8.4	1.003	0.974	**0.820**	0.025	—
SFRS2	Splicing factor, arginine/serine-rich 2	Q6PDU1	25.5/11.9	0.852	0.249	**0.826**	0.005	—
FEN1	Flap endonuclease 1	P39748[c]	42.6/8.8	0.971	0.775	**0.833**	0.022	23

[a] The average ratio of iTRAQ data with *p* value smaller than 0.05 is highlighted with bold font.
[b] The proteins with Refs. 22 and 23 had been reported previously as NGF-responsive genes at the mRNA level.
[c] Proteins identified with human taxonomy.
[d] Proteins identified with mouse taxonomy.

exact test). The annotation data of the 72 differentially expressed proteins were used to determine the overrepresented biological processes related to NGF-induced PC12 cell differentiation. A GO tree view composed of enriched biological processes in the up-regulated proteins was built according to the tree view in AmiGO, a tool for searching and browsing the Gene Ontology database (31).

Western Blotting—Cell lysate samples containing 20 μg of total protein were electrophoresed on SDS-polyacrylamide gels, transferred onto a PVDF membrane by electroblotting, and subjected to immunoblotting with the indicated antibody. In the case of prothymosin α (Pro$T\alpha$), cell lysate samples were transferred onto a membrane by electroblotting with acidic buffer (20 mM sodium acetate buffer, pH 5.2) followed by fixation with 0.5% glutaraldehyde (32, 33). Membranes were probed with different primary antibodies followed by horseradish peroxidase-conjugated mouse, rabbit, and goat secondary antibodies (GE Healthcare). The images were visualized with ECL (GE Healthcare). The following primary antibodies were used: neurosecretory protein VGF, CRMP-4, galectin-1, Pro$T\alpha$, MAGED1, and PCNA (Santa Cruz Biotechnology); plasminogen activator inhibitor 1 RNA-binding protein (PAIRBP1) (Abnova Co.); translationally controlled tumor protein (TCTP) (MBL International Corp.); β-actin (Sigma); peroxiredoxin 6 (Lab Frontier); and protein-disulfide isomerase (Stressgen). For the quantitative analysis, the ECL patterns were scanned using LabScan 5.0 (GE Healthcare) with transparent mode and a resolution of 300 dpi. The intensities were measured using ProGenesis Workstation Version 2005 (PerkinElmer Life Sciences).

Transfection of PC12 Cells with siRNA—Transfection of PC12 cells with siRNA was performed using Lipofectamine 2000 (Invitrogen) according to the manufacturer's protocol. Four target sequences for rat, PAIRBP1, TCTP, Pro$T\alpha$, and MAGED1 siRNA, were designed as follows. A 21-oligonucleotide siRNA duplex was designed as recommended elsewhere and was synthesized by Gene Link to target the PAIRBP1 sequence (5′-^{1125}AAGUGCUUCUGCUCCUGACTT-3′), the TCTP sequence (5′-^{357}AAGCACATCCTTGCTAATTTT-3′), the Pro$T\alpha$ sequence (5′-52AAGGAGAAGAAGGAAGUUGTT-3′), and the MAGED1 sequence (5′-^{1928}AAGUGCUGAGAUUCAUUGCTT-3′). A Silencer Negative Control siRNA 1 (Ambion) was used as a control siRNA for the analysis.

Immunofluorescence Analysis—PC12 cells cultured on 35-mm collagen-coated culture dishes were fixed with 4% paraformaldehyde in PBS for 15 min at room temperature and then permeabilized with 0.1% Triton X-100 in PBS on ice for 15 min. After being washed with PBS, cells were incubated in primary antibodies diluted in PBS containing 5% bovine serum albumin followed by anti-mouse or -rabbit Alexa Fluor® 488-conjugated IgG (Invitrogen) for 60 min at room temperature. After being washed with PBS, the cells were incubated for 10 min at room temperature with rhodamine-phalloidin (Invitrogen) to stain cellular F-actin. After being washed with PBS, the cells were incubated for 10 min at room temperature with 20 μg/ml Hoechst33342 (Invitrogen) to stain nuclear actin. Analysis was performed with a fluorescence microscope (with 20 × 1.6 Olympus IX71) (DPController, DPManager).

Quantification of Neurite Outgrowth—For quantification of the neurite outgrowth of PC12 cells, the cells transfected with siRNAs were cultured onto collagen-coated culture dishes (Iwaki) under the condition of 1% horse serum and stimulated with 50 ng/ml 2.5 S NGF (Wako) at 48 h. Total neurite length of NGF-stimulated PC12 cells was measured using MetaMorph software (Molecular Devices). The total number of tip ends was manually counted to represent the number of neurites from individual cells. For each measurement, at least 50 cells per dish were analyzed from randomly selected fields. Each experiment was repeated three times.

Evaluation of PC12 Cell Death—Propidium iodide (PI) was used for the evaluation of PC12 cell death. Cells transfected with siRNAs were cultured onto 35-mm collagen-coated culture dishes (Iwaki) under the condition of 10% horse serum and 5% fetal bovine serum and stimulated with 50 ng/ml 2.5 S NGF (Wako) at 48 h. The cells were fixed with 4% paraformaldehyde in PBS and incubated with 0.2 μg/ml PI for apoptotic cells and 20 μg/ml Hoechst33342 (Invitrogen) for total cells for 10 min at room temperature. PI-positive cells were counted using a fluorescence microscope (with 20 × 1.6 Olympus IX71) (DPController, DPManager). For each counting, at least 500 cells per dish were counted from randomly selected fields. Each experiment was repeated three times.

Time Lapse Video Analysis—Cells were cultured on a collagen-coated glass bottom plate with 6 wells (Iwaki). The plate was main-

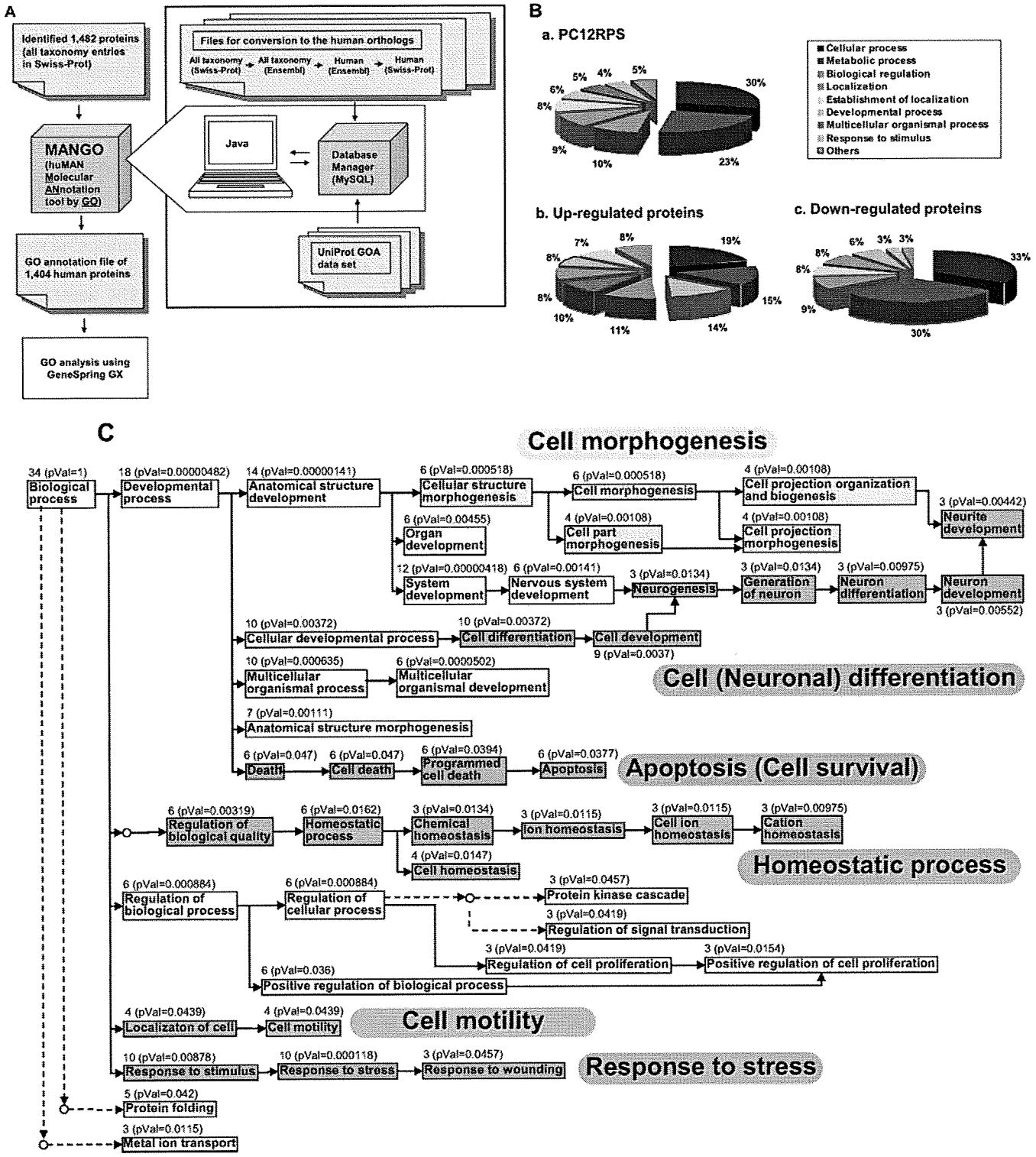

FIG. 3. **GO analysis of PC12 proteins differentially expressed after NGF stimulation.** *A*, work flow for proteomics GO analysis (MANGO method). MANGO (a Web application), composed of the mySQL 4.0 and scripts written in Java, automatically executed the following steps. First, 1,482 proteins with multiple species matches were converted to human orthologs according to the conversion steps using Ensembl Mart files shown in the figure. Then the converted human orthologs were annotated with GO according to the UniProt GOA data set (described under "Experimental Procedures"). The resulting list of 1,404 GO-annotated human proteins was used as the PC12PRS as shown in supplemental Table 4. GeneSpring GX was used to determine statistically overrepresented GO categories from the iTRAQ data set. *B*, classification by annotated biological processes of the PC12PRS (*a*), 39 up-regulated (*b*), and 33 down-regulated (*c*) proteins identified with the iTRAQ method.

tained at 37 °C under the air condition of 5% CO_2 in the chamber set under the camera during the observation. Images were obtained by using a 20× UPlan SApo objective (Olympus IX81). The camera, shutters, and filter wheel were controlled by MetaMorph imaging software (Molecular Devices), and the images were collected every 10 min with an exposure time of 50 ms.

RESULTS

Identification of Differentially Expressed Proteins in Response to NGF in PC12 Cells—For the fourplex iTRAQ labeling, four independent, separately cultured cell lysates were prepared in parallel. The tryptic peptides from untreated cells were labeled with mass 114 and 115 isobaric iTRAQ tags, and those from NGF-treated cells were labeled with mass 116 and 117 isobaric iTRAQ tags. The iTRAQ-labeled peptides were then fractionated by cation exchange column chromatography and analyzed with LC-MS/MS using both MALDI and ESI (Fig. 1).

With LC-MALDI-MS/MS, 1,324 proteins were identified from 14,710 peptide sequences; in contrast, with LC-ESI-MS/MS, 902 proteins were identified from 12,769 peptide sequences. Only 744 proteins were identified by both systems, and 580 and 158 proteins were uniquely identified with LC-MALDI-MS/MS and LC-ESI-MS/MS, respectively. In total, 1,482 proteins were identified with >95% confidence (Fig. 2*A* and supplemental Table 1). At a -fold change of >20% (ratio >1.20 or <0.83), 15 proteins identified with LC-MALDI-MS/MS were up-regulated, and 19 were down-regulated, whereas 32 identified with LC-ESI-MS/MS were up-regulated, and 18 were down-regulated (p value <0.05) (Fig. 2, *B* and *C*). Eight up- and four down-regulated proteins were identified by both systems, and seven or 24 up- and 15 or 14 down-regulated proteins were uniquely identified with LC-MALDI-MS/MS or LC-ESI-MS/MS, respectively (Fig. 2, *B* and *C*). In total, 72 proteins (39 up- and 33 down-regulated) were differentially expressed in response to NGF. Among the NGF-responsive proteins, 64 were newly identified in this study (Table I and supplemental Tables 2 and 3).

Proteomics GO Analysis of NGF-responsive Proteins—The list of differentially expressed proteins was prepared for use in GO analysis with GeneSpring using a new, in-house taxonomy conversion/GO annotation tool, MANGO (a Web application) (Fig. 3*A*). First the taxonomies of all 1,482 identified proteins (multiple species matches) were converted to the *Homo sapiens* taxonomy. 1,404 of them were assigned human orthologs and annotated with GO information from UniProt. This GO-annotated list, compiled using the MANGO tool, was designated as the PC12 proteome reference set (PC12PRS) on which two distinct proteomics GO analyses were subsequently performed (supplemental Table 4). In the first analysis, to determine the overrepresented biological processes specifically related to the NGF-induced PC12 cell differentiation, we simply compared the GO categories represented by the differentially expressed proteins in the PC12PRS with the GO categories represented by the PC12PRS overall (Fig. 3*B*). From this we found that the following biological processes occurred significantly more frequently in the GO annotations of the 39 up-regulated proteins than they did in the PC12PRS as a whole: "developmental process" (14 *versus* 6%), "multicellular organismal process" (10 *versus* 5%), and "response to stimulus" (8 *versus* 4%) (Fig. 3*B*, *a* and *b*). Also on the other hand, the occurrence ratio of "metabolic process" (30 *versus* 23%) was higher in the GO annotations of the 33 down-regulated proteins than in those of the PC12PRS as a whole (Fig. 3*B*, *a* and *c*). Next to obtain further statistical interpretation, a second proteomics GO analysis of the differentially expressed proteins in the PC12PRS (supplemental Table 4) was performed to determine which biological processes were enriched in the 39 up-regulated and the 33 down-regulated proteins (Table II). Using these data, a GO tree view was built to clarify the interrelationships of these biological processes (Fig. 3*C*). The part of the tree comprising the up-regulated proteins was mainly divided into six branches, which included "cell morphogenesis" (p value = 0.000518), "apoptosis (cell survival)" (p value = 0.0377), "homeostatic process" (p value = 0.0162), "cell motility" (p value = 0.000118), "response to stress" (p value = 0.000118), and "cell differentiation" (p value = 0.00372) (Tables II and III and Fig. 3*C*). On the other hand, the part of the tree comprising the down-regulated proteins included cellular metabolic processes, especially RNA and DNA metabolic processes (Tables II and III).

Biological Validation of Newly Identified NGF-responsive Proteins Related to GO Categories Extracted by MANGO—Of the six up-regulated groups listed in Table II, we focused on cell morphogenesis and apoptosis/cell survival (Fig. 3*C* and Table III) and used a time course analysis by Western blotting to study the expression patterns of the up-regulated proteins related to these processes (Fig. 4). Neurosecretory protein VGF, the most significantly up-regulated protein identified by both LC-MALDI-MS/MS and LC-ESI-MS/MS (Table I and supplemental Fig. 1), was used as a positive control of the time-dependently increased protein by Western blotting (Fig. 4). Seven proteins, CRMP-4, MAGED1, PAIRBP1, protein-disulfide isomerase, peroxiredoxin 6, ProTα, and TCTP, were up-regulated in response to NGF with different expression patterns in the time course study (Fig. 4, *A* and *B*, and supplemental Fig. 2). Interestingly TCTP and MAGED1 expression

C, a GO hierarchy tree of biological processes annotating the 39 up-regulated proteins. GO analysis was performed by using GeneSpring GX software. A GO tree view composed of enriched biological processes in the up-regulated proteins was built according to the tree view in AmiGO. Direct and indirect hierarchies are indicated by *full* and *dotted lines* with *arrows*, respectively. The number of molecules and p values (*pVal*) for biological processes annotated are shown in the tree.

TABLE II

Overrepresented biological processes by proteomics GO analysis of proteins differentially expressed in response to NGF stimulation

Categories	All proteins in category	Percentage of all proteins in category	Up- or down-regulated proteins in category	Percentage of up- or down-regulated proteins in category	*p* value
Up-regulated proteins					
GO:8150: biological process	1,245	100	34	100	1
GO:32502: developmental process	231	18.55	18	52.94	4.82*e*−06
GO:48856: anatomical structure development	126	10.12	14	41.18	1.41*e*−06
GO:32501: multicellular organismal process	186	14.94	13	38.24	0.000635
GO:48731: system development	99	7.952	12	35.29	4.18*e*−06
GO:7275: multicellular organismal development	125	10.04	12	35.29	5.02*e*−05
GO:6950: response to stress	95	7.631	10	29.41	0.000118
GO:48869: cellular developmental process	145	11.65	10	29.41	0.00372
GO:30154: cell differentiation	145	11.65	10	29.41	0.00372
GO:50896: response to stimulus	163	13.09	10	29.41	0.00878
GO:48468: cell development	121	9.719	9	26.47	0.0037
GO:9653: anatomical structure morphogenesis	63	5.06	7	20.59	0.00111
GO:32989: cellular structure morphogenesis	40	3.213	6	17.65	0.000518
GO:902: cell morphogenesis	40	3.213	6	17.65	0.000518
GO:7399: nervous system development	48	3.855	6	17.65	0.00141
GO:65008: regulation of biological quality	56	4.498	6	17.65	0.00319
GO:48513: organ development	60	4.819	6	17.65	0.00455
GO:48518: positive regulation of biological process	93	7.47	6	17.65	0.036
GO:6915: apoptosis	94	7.55	6	17.65	0.0377
GO:12501: programmed cell death	95	7.631	6	17.65	0.0394
GO:8219: cell death	99	7.952	6	17.65	0.047
GO:48523: negative regulation of cellular process	99	7.952	6	17.65	0.047
GO:16265: death	99	7.952	6	17.65	0.047
GO:6457: protein folding	72	5.783	5	14.71	0.042
GO:30030: cell projection organization and biogenesis	18	1.446	4	11.76	0.00108
GO:48858: cell projection morphogenesis	18	1.446	4	11.76	0.00108
GO:32990: cell part morphogenesis	18	1.446	4	11.76	0.00108
GO:19725: cell homeostasis	36	2.892	4	11.76	0.0147
GO:42592: homeostatic process	37	2.972	4	11.76	0.0162
GO:6928: cell motility	50	4.016	4	11.76	0.0439
GO:51674: localization of cell	50	4.016	4	11.76	0.0439
GO:31175: neurite development	13	1.044	3	8.824	0.00442
GO:48666: neuron development	14	1.124	3	8.824	0.00552
GO:30003: cation homeostasis	17	1.365	3	8.824	0.00975
GO:30182: neuron differentiation	17	1.365	3	8.824	0.00975
GO:6873: cell ion homeostasis	18	1.446	3	8.824	0.0115
GO:30001: metal ion transport	18	1.446	3	8.824	0.0115
GO:50801: ion homeostasis	18	1.446	3	8.824	0.0115
GO:22008: neurogenesis	19	1.526	3	8.824	0.0134
GO:48699: generation of neurons	19	1.526	3	8.824	0.0134
GO:48878: chemical homeostasis	19	1.526	3	8.824	0.0134
GO:8284: positive regulation of cell proliferation	20	1.606	3	8.824	0.0154
GO:9966: regulation of signal transduction	29	2.329	3	8.824	0.0419
GO:42127: regulation of cell proliferation	29	2.329	3	8.824	0.0419
GO:7243: protein kinase cascade	30	2.41	3	8.824	0.0457
GO:9611: response to wounding	30	2.41	3	8.824	0.0457
Down-regulated proteins					
GO:8150: biological process	1,245	100	29	100	1
GO:44237: cellular metabolic process	824	66.18	24	82.76	0.0386
GO:43283: biopolymer metabolic process	389	31.24	15	51.72	0.0161
GO:61 nucleobase, nucleoside, nucleotide, and nucleic acid	337	27.07	14	48.28	0.011
GO:6397: mRNA processing	86	6.908	7	24.14	0.00263
GO:16071: mRNA metabolic process	101	8.112	7	24.14	0.0066
GO:6396: RNA processing	107	8.594	7	24.14	0.00907
GO:8380: RNA splicing	86	6.908	6	20.69	0.0119
GO:6259: DNA metabolic process	70	5.622	5	17.24	0.0201
GO:6281: DNA repair	23	1.847	3	10.34	0.0147
GO:6974: response to DNA damage stimulus	25	2.008	3	10.34	0.0185
GO:9719: response to endogenous stimulus	27	2.169	3	10.34	0.0228

TABLE III
The differentially expressed proteins related to the enriched biological processes

GO categories	Protein name (abbreviation)[a]
Up-regulated proteins	
Cell differentiation	SQSTM, RAC1, MAP1B, ENPL, CROP, NEUM, GAL1, TCTP, SCG2, S100A6, PROTA,[b] PAIRBP1[b]
Response to stress	RAC1, SQSTM, ENPL, DNJA1, CROP, AT1A1, SCG2, ANXA2, OXRP, PRDX6
Cell morphogenesis	RAC1, RADI, S100A6, ENOA, NEUM, MAP1B, MAGED1,[b] CRMP4[b]
Apoptosis (cell survival)	SQSTM, ENPL, TCTP, CROP, LEG1, SCG2, PAIRBP1,[b] MAGED1,[b] PROTA[b]
Homeostatic process	ENPL, AT1A1, PDI, TCTP,
Cell motility	MOES, AT1A1, SGTA, RAC1
Down-regulated proteins	
DNA and RNA metabolic process	HNRLL, SRR35, LSM8, FUBP2, HNRPF, SFRS2, PRP19, PCNA, H2B1C, H2B2A, FEN1
Other cellular metabolic process	VTDB, TBB4, GALK1, RL34, UBP48, CSK21, RLA0, IDHP, TIM13, PRPS2, DDC, RL6, APT

[a] The abbreviation of the protein name listed in Table I are shown in this table.
[b] These proteins were not annotated with the enriched biological processes, but they are speculated to be related to the biological process as reported in Refs. 34 and 35 for PAIRBP1, in Ref. 37 for PROTA, in Ref. 38 for MAGED1, and in Ref. 55 for CRMP4.

increased for 12 h and then gradually decreased. On the other hand, galectin-1 and ProTα expression levels peaked at 48 and 24 h, respectively. CRMP-4 and PAIRBP1 expression levels were constantly up-regulated during 12–72 h of NGF stimulation. The down-regulated protein, PCNA, was also consistently regulated in response to NGF (Fig. 4*A*). PAIRBP1 (34, 35), TCTP (36), ProTα (37), and MAGED1 (38) have been speculated to be functionally related to cellular differentiation and survival/apoptosis. We therefore sought to identify the roles of these proteins. Immunocytochemistry (ICC) showed that PAIRBP1 was expressed not only in the cytoplasm but also in the neurites, especially at the tips and junctions (Fig. 5*A*, *g* and *i*, *arrowheads*), whereas MAGED1 was expressed only in the cytoplasm (Fig. 5*D*, *g* and *i*). TCTP and ProTα were strongly expressed in the nucleus in response to NGF (Fig. 5, *B* and *C*, *g* and *i*, *arrows*). These results suggested that those proteins were involved in NGF-treated cellular responses.

Suppression of Differentially Expressed Proteins by siRNA Treatment—PAIRBP1, TCTP, ProTα, and MAGED1 were further analyzed using specific siRNAs to investigate their functions. siRNA-induced down-regulation was confirmed by Western blotting and ICC using their specific antibodies (Fig. 6, *A* and *B*) followed by a test of whether or not their suppression morphologically influenced the PC12 neurite formation. As expected, significant inhibition of the neurite formation was observed (Fig. 6*B*). Interestingly the suppression of MAGED1 caused aggregation of differentiating cells (Fig. 6, *B*, *IV* and *C*, *a*, and supplemental Movie 5). Furthermore we calculated the number and total length of neurites in differentiating cells and found that these measurements were certainly decreased by the suppression of each protein (Fig. 6*C*, *b* and *c*). In addition, apoptotic phenotypes were observed in NGF-stimulated cells treated with PAIRBP1, TCTP, or ProTα siRNA (Fig. 6*C*, *a* and supplemental Movies 2–4). We therefore observed the effects of the down-regulation of these proteins by siRNA on the survival of NGF-treated PC12 cells using PI staining for apoptotic cells coupled with nuclear staining by Hoechst33342. PAIRBP1, TCTP, or ProTα suppression caused a significant increase in PI-positive cells, whereas suppression of MAGED1 did not (Fig. 6*C*, *d* and *e*). These results suggested that, in PC12 cells, PAIRBP1, TCTP, ProTα, and MAGED1 regulate NGF-induced differentiation and that, except for MAGED1, they are involved in cell survival.

DISCUSSION

MS-based techniques targeting functional proteins in biological specimens have been developed to improve sensitivity, quantitation, and throughput. However, their application to biological study has not been satisfactory because their independent development has not met the needs of cell biologists and because of the lack of a sequential protocol and associated user-friendly analysis tools. Here we present a concise strategy consisting of sequential MS-based, *in silico*, and cell biological analyses to study the mechanisms of neuronal differentiation using PC12 cells.

Using MALDI-TOF-TOF and ESI-QqTOF in parallel, not only were certain proteins identified by both methods, but also unique proteins were independently identified by either of the methods. These data were combined to increase the number of identified proteins. It seemed important to know what kind of differences there were between the unique peptides identified by either of the systems. Previously Stapels and Barofsky (39) reported that the ESI system favored the identification of hydrophobic peptides whereas the MALDI system tended to lead to the identification of basic and aromatic peptides in the analysis of *E. coli* DNA-binding proteins. We noticed that the peptides identified by ESI-QqTOF had relatively higher theoretical pI values and molecular weights (pI = 6.46 and M_r = 1,694.4 on average) compared with those identified by MALDI-TOF-TOF (pI = 5.81 and M_r = 1,651.6 on average). The discrepancy, which seems contradictory, between our results and those of Stapels and Barofsky (39) may be explained by differences in sample, type of proteins analyzed, and the presence or absence of modification such as iTRAQ

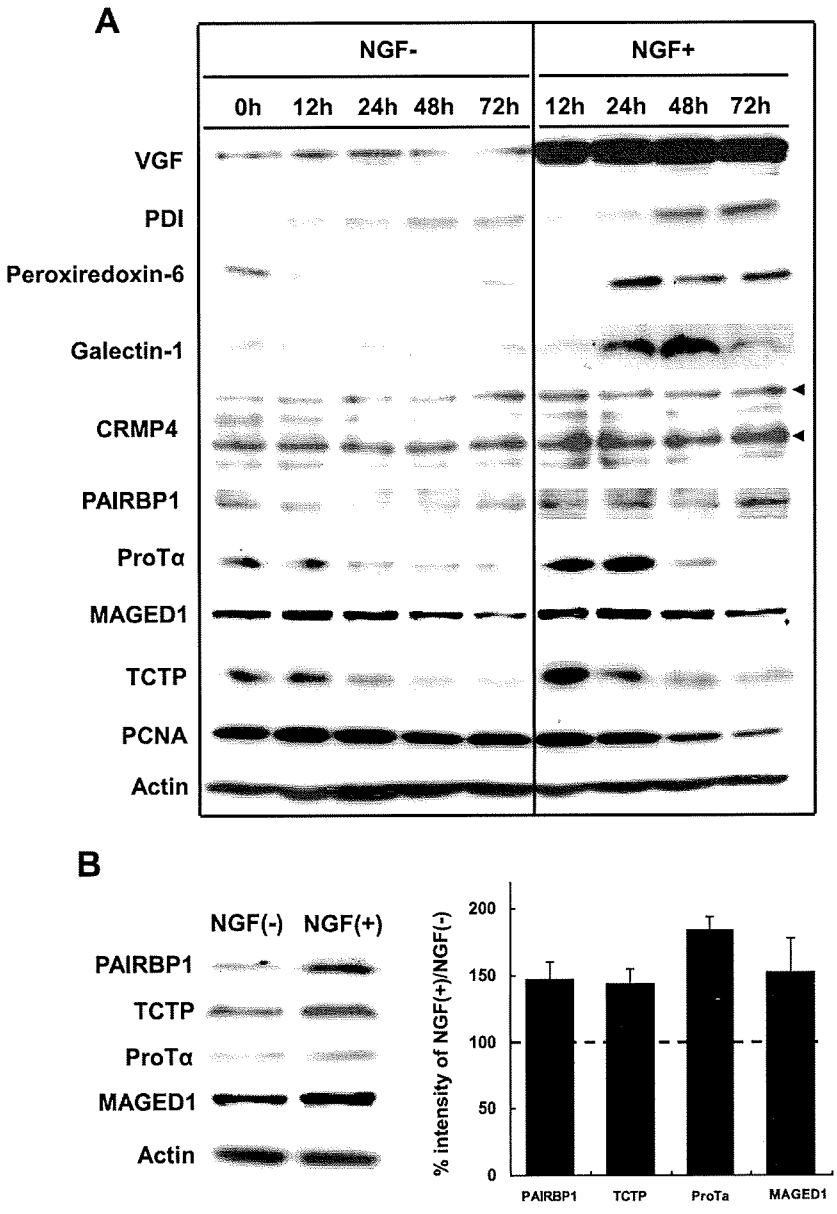

FIG. 4. **Immunoblot images of PC12 proteins differentially expressed in response to NGF stimulation.** Cell lysates were prepared at different time points as indicated. Actin expression was assessed for equal loading for all the proteins. *A*, the representative images are shown in four reproducible experiments. *Upper* and *lower arrowheads* show isoforms 1 and 2 of CRMP4, respectively. Some of those proteins showed a change in their expression levels even in untreated cells probably because of certain signals from collagen coated on the plates. *B*, Western blot images and quantification of the above four proteins PAIRBP1, TCTP, ProTα, and MAGED1 in NGF-stimulated PC12 cells. Cell lysates were prepared at 48 h after NGF stimulation. Actin expression was assessed for equal loading for all the proteins. The representative images are shown in four reproducible experiments. The ratios of percent intensities of the four proteins in NGF-stimulated *versus* untreated PC12 obtained from four separate identical experiments are shown in the histogram. *Error bars* represent S.D. The ratios were largely consistent with the corresponding iTRAQ ratios.

labeling. These results suggest that both MS systems may be complementary due to the biases of the two ionization systems and that analyses should be performed using both instruments to obtain more comprehensive information out of a given set of samples in a proteomics study.

In total, we analyzed 1,482 proteins with iTRAQ quantitation data of 4,899 proteins from 40,037 peptides identified by using the Mascot search engine (data not shown) in this study. To understand how our identification strategy covers the proteins expressed in PC12 cells, we analyzed the cellular component locations of all the identified proteins by the MANGO method and compared them with those of all human proteins listed in the Swiss-Prot database (20,332 entries, Release 57.2 of May 5, 2009) (supplemental Table 5). Of the 1,404 total identified human orthologs (PC12RPS), 1,231 were annotated with cellular component data. Of the latter, 758 (62%), 166 (13%), and 118 (10%) proteins were annotated with "cytoplasm," "mitochondrion," and "plasma membrane," respectively. On the other hand, among 16,530 human proteins from the Swiss-Prot database annotated with cellular component data, 7,106 (43%), 1,033 (6%), and 3,632 (22%) proteins were annotated with cytoplasm, mitochondrion, and plasma membrane, respectively. In the PC12RPS, the occurrence ratios of cytoplasm (62%) and mitochondrion (13%) were higher than those in the Swiss-Prot human proteins (43 and 6%, respectively), whereas the ratio of plasma membrane (10%) in PC12RPS was lower than that in the Swiss-Prot human proteins (22%). By combining this ratio of plasma membrane with the ratio of "organelle membrane" proteins (10.97%), the percentage of membrane proteins in the total proteins identified

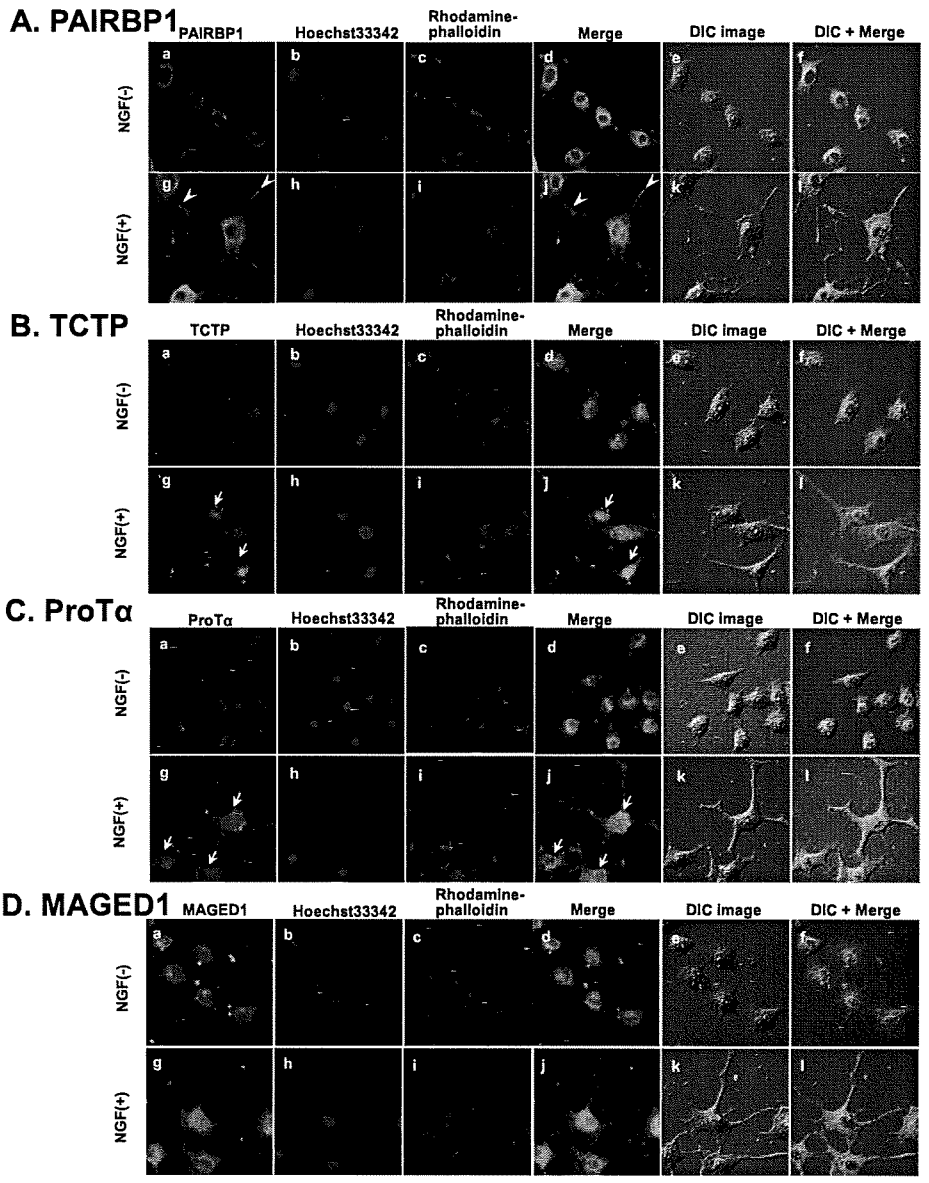

FIG. 5. **Analysis of NGF-responsive proteins by ICC.** PC12 cells were treated with NGF for 48 h. Cells were fixed and incubated with antibodies against the indicated proteins (*A*, PAIRBP1; *B*, TCTP; *C*, ProTα, and *D*, MAGED1) followed by detection with Alexa Fluor 488-labeled secondary antibodies (*a* and *g*) and observation with a fluorescence microscope. Nuclear and F-actin were stained with Hoechst33342 (*b* and *h*) and rhodamine-phalloidin (*c* and *i*), respectively. The merged images for *a*, *b*, *c* and *g*, *h*, *i* are shown in *d* and *j*, respectively. The merged images for *d*, *e* and *j*, *k* are shown in *f* and *l*. Differential interference contrast (*DIC*) images of PC12 cells in the same field are shown in *e* and *k*. *Arrowheads* indicate the PAIRBP1 expression in the neurite junctions and tips. *Arrows* indicate the TCTP and ProTα expression in the nucleus.

in our study becomes more than 20%. From these results, it is suggested that although cytoplasmic and mitochondrial proteins are largely favored in our method other components such as membrane and nuclear proteins can be also identified in significant numbers (supplemental Table 5).

From 1,482 proteins identified in iTRAQ quantitation, 72 differentially expressed proteins, including 39 up-regulated and 33 down-regulated, were extracted. The up-regulation of neurosecretory protein VGF (40), neuromodulin (41), chromogranin A (42), annexin A2 (43), peripherin (44), MAP1B (45), AHNAK (46), and secretogranin 2 (42) was observed as reported previously (Table II). Eighteen proteins in our results also corresponded to NGF-responsive genes in cDNA microarray data of Dijkmans *et al.* (23) (Table II) that coincided with our results, showing the confidence and reliability of our methods. Sixty-four proteins were heretofore unreported (Table II). The majority were cytoskeletal organizing components, such as moesin, radixin, MAP1B, annexin A2, peripherin, CRMP-4, RAC1, keratin-8, and keratin-18, whose changes in expression suggested roles for them in the cytoskeletal reorganization for cellular motility and morphogenesis. Interestingly PCNA and flap endonuclease 1 are both required for DNA replication, and both histones H2A and H2B are nucleosome components, all of which were down-regulated by NGF treatment. These results suggested that the down-regulation of these proteins was a factor in the arrest of cell division and the initiation of PC12 neuronal differentiation.

Further biological and functional interpretation of the above proteins was performed by proteomics GO analysis using the GO annotation and analysis tool. Here we encountered two problems. First, unlike microarray data, proteomics data con-

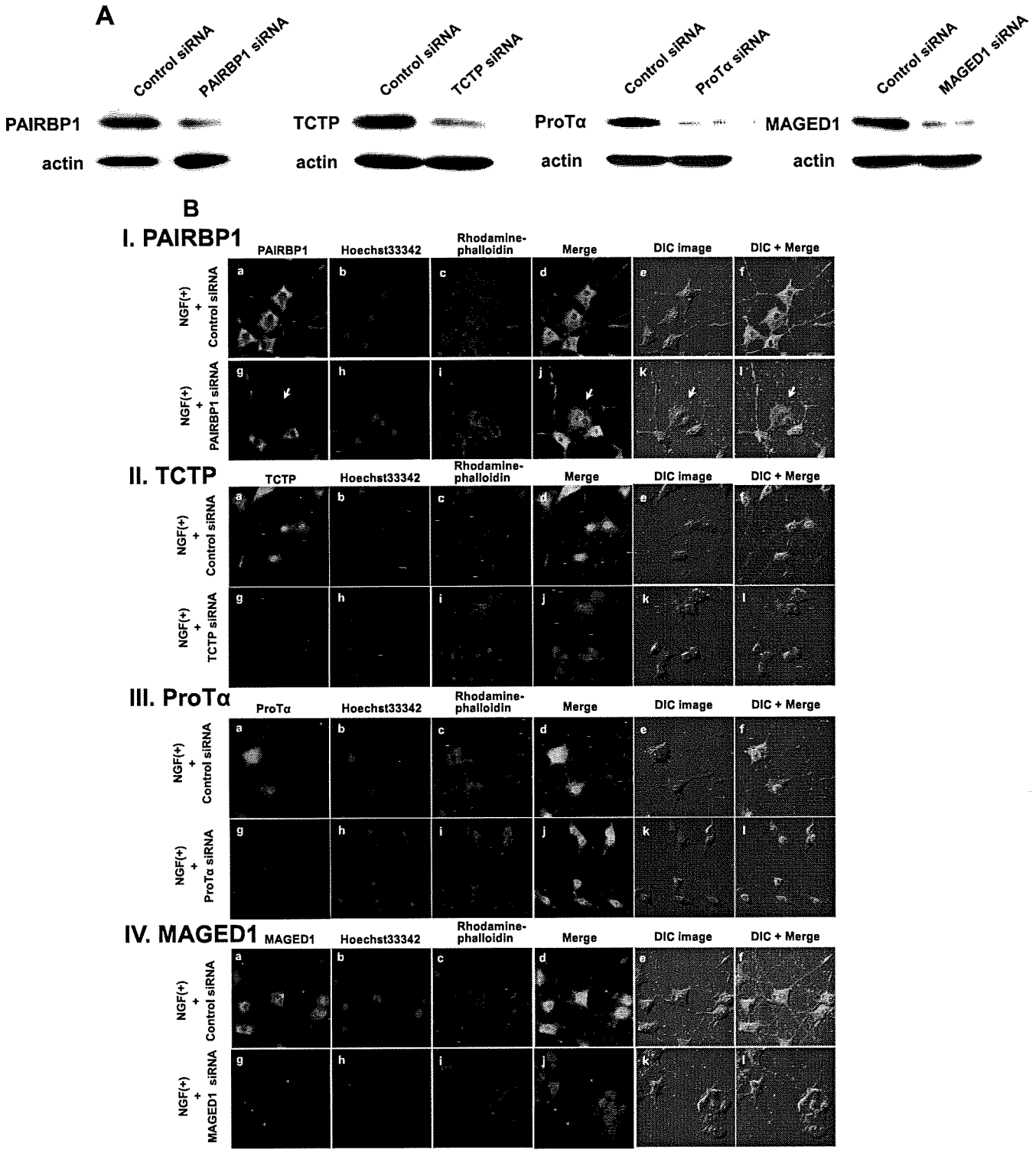

FIG. 6. **The effects caused by the suppression of the NGF-inducible proteins on PC12 cell differentiation.** *A*, the cells were transfected with siRNA for each NGF-inducible protein or control siRNA for 24 h and then treated with NGF for 48 h. Immunoblot images were taken after treatment with each siRNA of the protein. Down-regulation of these proteins was confirmed. *B*, the cells were transfected with siRNA for each NGF-inducible protein or control siRNA for 24 h and then treated with NGF for 48 h. Cells were fixed and incubated with the antibodies against the indicated proteins (*I*, PAIRBP1; *II*, TCTP; *III*, ProTα; and *IV*, MAGED1) followed by detection with Alexa Fluor 488-labeled secondary antibodies and observation with a fluorescence microscope (*a* and *g*). Nuclear and F-actin were stained with Hoechst33342 (*b* and *h*) and rhodamine-phalloidin (*c* and *i*), respectively. The merged images for *a*, *b*, *c* and *g*, *h*, *i*, are shown in *d* and *j*, respectively. The merged images

sisting of thousands of proteins cannot be easily annotated by GO because of the general lack of either an automated method of proteomics GO annotation or GO analysis software that directly links to the proteomics database. Second, the genome information (including GO) of rat is much poorer than that of human or mouse. To overcome those difficulties, we therefore created a simple method, namely the MANGO method, that consists of the annotation tool (MANGO) and our PC12 cell proteome reference set (PC12RPS) with all non-human proteins converted into corresponding human orthologs. This method enabled us to analyze the GO of the differentially expressed proteins using the human PC12RPS very quickly.

The MANGO method helped us to narrow the focus of our study when the results suggested that NGF-induced PC12 cell differentiation involves functional up-regulation of protein groups related to six processes from which we selected cell morphogenesis and apoptosis/cell survival for deeper investigation. This led to biological validation by Western blotting, which confirmed that all of proteins in these groups were in fact up-regulated in PC12 cells by the NGF treatment (Fig. 4). Because their neuronal functions have not been reported in detail, of the proteins shown in Fig. 4, we focused on PAIRBP1 (34, 35), TCTP (36), ProTα (37), and MAGED1 (38). The indispensable roles of these proteins were further indicated by our subsequent ICC and siRNA-based studies. In this way, our MANGO method allowed us to quickly determine high probability candidate proteins whose important roles in NGF-induced PC12 cell differentiation are elaborated below.

PAIRBP1 has been identified as a protein involved in the regulation of PAI-1 mRNA stability via its binding to the cyclic nucleotide-responsive sequence of the PAI-1 mRNA (34). PAI-1 is the primary inhibitor of both urokinase- and tissue-type plasminogen activator (47). Soeda *et al.* (35) have shown that PAI-1 promotes the neurite outgrowth and survival of PC12 cells. This neuroprotective activity is correlated with enhanced activation of both extracellular signal-regulated kinase following a direct phosphorylation of NGF receptor Trk A and c-Jun, suggesting that PAI-1 can act as a neurotrophic factor (35). Based on those findings, we hypothesized that PAIRBP1 would be a positive regulator of PC12 differentiation and survival via PAI-1 mRNA stability. In our study, we observed that its suppression caused the inhibition of neurite formation and cell death. Interestingly PAIRBP1 was expressed not only in the cytoplasm but also in the neurites, especially in the tips and junctions (Fig. 5*A*, *g* and *i*, *arrowheads*), suggesting that it may have some other essential roles such as in cytoskeletal reorganization for the neurite formation that are independent of PAI-1.

TCTP has been identified in many eukaryotes and is widely expressed. It is a growth-related protein whose expression is highly regulated at the transcriptional and translational levels and by a wide range of extracellular signals (48). TCTP is involved in calcium binding and microtubule stabilization and is implicated in the regulation of cell growth and the cell cycle (48). It is also postulated to have antiapoptotic activity (49). Previous reports have revealed that TCTP protein expression decreased in differentiating mouse embryonic stem cells (mESCs) (50) and in dopaminergic motor neurons having differentiated from mouse E14 cells (36), indicating that TCTP has an important role in mESC differentiation. In contrast, in our iTRAQ data, TCTP was up-regulated after 48 h of NGF stimulation. Our Western blotting analysis showed the time-dependent changes of the TCTP intensity after NGF treatment; namely the intensities had increased up to 12 h and then gradually decreased. This TCTP expression pattern in NGF-treated PC12 cells seems to be similar to that of the developing mESC. Compared with the TCTP intensities without NGF, those with NGF were higher throughout the same analysis (12–72 h) (Fig. 4 and supplemental Fig. 2). We also showed in this study that TCTP knockdown caused inhibition of neurite formation and apoptosis (Fig. 6*C*), suggesting that NGF-induced up-regulation of TCTP could be a trigger of neurite outgrowth and that its down-regulation after this triggering role might have another function in the neurite formation or cell survival of NGF-induced PC12 cells.

ProTα is a highly acidic protein widely expressed in mammalian cells. ProTα gene expression is correlated with cell

for *d*, *e* and *j*, *k* are shown in *f* and *l*, respectively. Differential interference contrast (*DIC*) images of PC12 cells in the same field were shown in *e* and *k*. The suppression of expression of each protein led to significant morphological changes, such as inhibition of neurite formation and induction of cellular aggregation in differentiating PC12 cells. *Arrowheads* indicate the PAIRBP1-suppressed cells. *C*, effects on neurite outgrowth and survival of PC12 cells of the siRNA treatment of the NGF-inducible proteins. *a*, representative time lapse images of NGF-stimulated PC12 cells treated with each siRNA for NGF-inducible proteins. The cells were transfected with siRNA for each NGF-inducible protein or control siRNA and stimulated with NGF for 72 h. A significant inhibition of neurite formation was observed due to each siRNA treatment. *Arrows* show the apoptotic phenotypes of PC12 cells. *b* and *c*, the cells were transfected with siRNA for each NGF-inducible protein or control siRNA and stimulated with NGF for 48 h under the condition of low serum (1% horse serum). The average of the number and total length of neurites of the PC12 cells are shown on the *y axis* (*b* and *c*). The data are expressed as means and S.D. of the three independent experiments ($n = 3$). For each experiment, more than 50 cells were counted. *d* and *e*, effects on PC12 cell survival of the siRNA treatment of the NGF-inducible proteins. The cells were transfected with siRNA for each NGF-inducible protein or control siRNA, stimulated with NGF for 48 h, fixed, and stained with PI and Hoechst33342 dye. Representative images of PI and Hoechst staining of PC12 cells treated with each siRNA and control and stimulated with NGF are shown (*d*). The percentage of PI-positive PC12 cells in total Hoechst-stained PC12 cells is shown on the *y axis* (*e*). The data and *error bars* are expressed as means and S.D. of the three independent experiments ($n = 3$), respectively. For each experiment, more than 500 cells were counted. *, $p < 0.05$; **, $p < 0.01$; and ***, $p < 0.001$ *versus* NGF + control siRNA treatment (Student's *t* test).

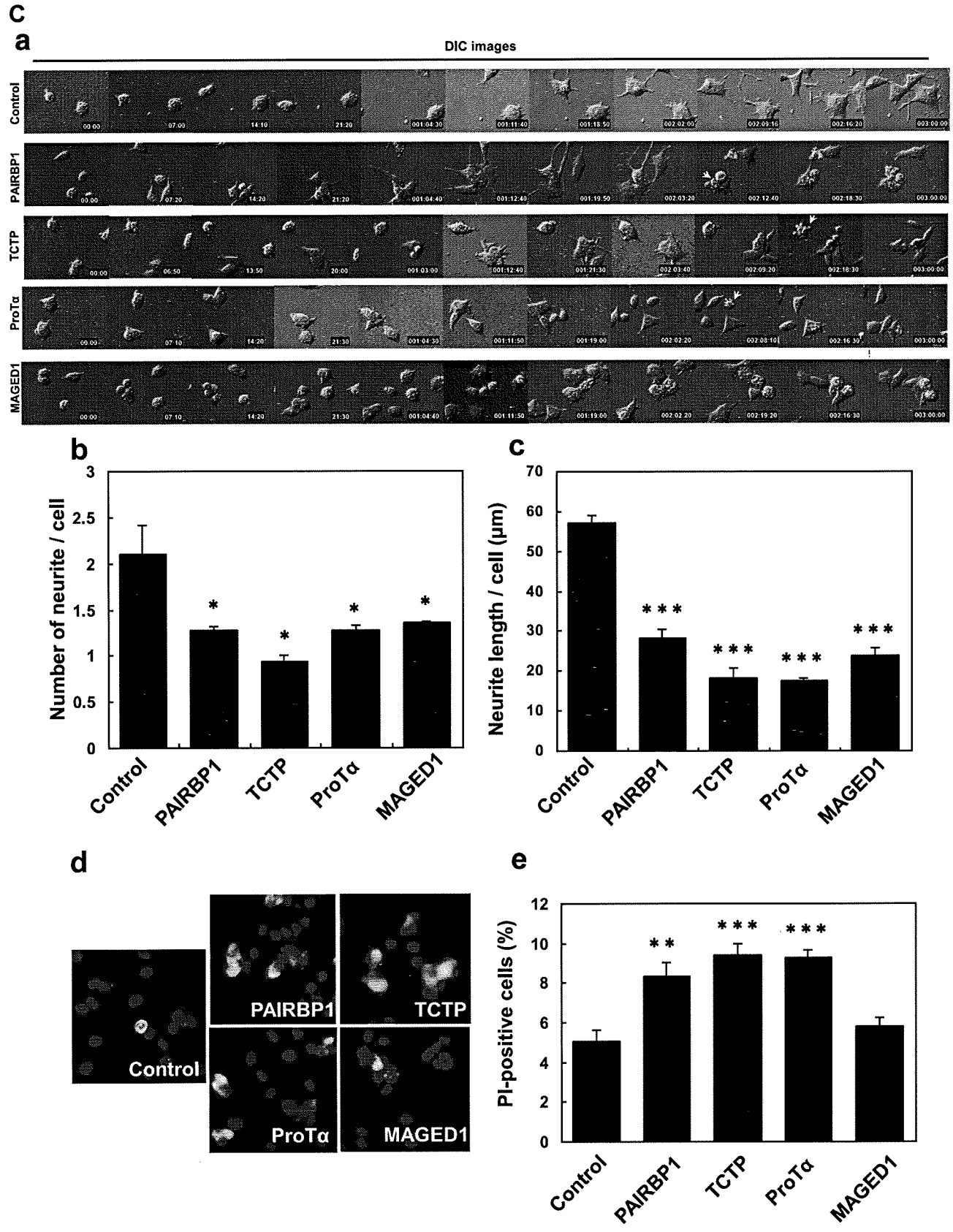

FIG. 6—*continued*

proliferation in a wide variety of cells, providing evidence for its involvement in cell growth (51). ProTα overexpression has been shown to both accelerate proliferation and retard differentiation in several cell types, such as HL60, K562, U937, and PC12 (37). Because ProTα was up-regulated in our proteomics analysis, we evaluated the time-dependent change in ProTα protein levels after NGF treatment by Western blotting (Fig. 4 and supplemental Fig. 2). ProTα expression peaked at 24 h and was followed by immediate down-regulation, suggesting that there might be some strict feedback mechanisms for ProTα expression in NGF-induced PC12 differentiation. Also ProTα was primarily localized in the nucleus after NGF stimulation (Fig. 5*C*, *g* and *i*, *arrows*). Nuclear ProTα reportedly interacts with histone H1 to promote chromatin decondensation and facilitate transcription or replication, the mechanism of which is regulated by casein kinase II phosphorylation of ProTα (52). Interestingly we observed that the expression of the casein kinase II catalytic subunit was down-regulated by NGF (Table I). The up-regulation of ProTα with accompanying casein kinase II down-regulation could therefore lead to transcriptional activation of genes related to PC12 cell differentiation and survival.

MAGED1, neurotrophin receptor-interacting MAGE homolog, was identified as a binding partner for p75 neurotrophin receptor (p75NTR) by yeast two-hybrid assay (38). MAGED1 reportedly binds p75NTR, antagonizes p75NTR to TrkA association, inhibits cell cycle progression, and facilitates p75NTR-mediated apoptosis (38). However, there is little information about p75NTR-mediated signaling by MAGED1. Because the localization of MAGED1 is not consistent with that of p75NTR (53), MAGED1 is likely to have the potential for signaling that is independent of p75NTR. Human MAGED1 reportedly regulates homotypic cell-cell adhesion by disrupting the E-cadherin·β-catenin complex (54). We observed the aggregation of differentiating PC12 cells triggered by the siRNA-induced MAGED1 down-regulation (Fig. 6, *B*, *IV* and *C*, *a*, and supplemental Movie 5), suggesting that MAGED1 suppression may have a significant effect on cell morphogenesis rather than cell survival during NGF-induced differentiation in PC12 cells.

In this study, we constructed the proteome database for PC12 cells containing the maximum number of the peptides/proteins so far identified and successfully identified new proteins related to cellular differentiation and apoptosis/survival. Our sequential proteomics strategy demonstrated here is simple and effective for identifying the proteins most likely involved in the physiological phenomena of interest because it enables one to quickly but confidently identify an appropriate focus on biological processes when interpreting extensive proteomics data. We expect that this proteomics strategy can become a standard method to target and elucidate the functions of proteins involved in cellular biological processes, to study the onset and pathogenesis of various diseases, and to discover new drug candidates in the near future.

Acknowledgments—We thank Prof. Hideyuki Saya, Keio University, School of Medicine, for kind advice and encouragement throughout this study. We also thank the entire staff of the Department of Tumor Genetics and Biology in Kumamoto University for helpful support, especially N. Tsubota, U. Midorikawa, and M. Nagayama for collaborative endeavors and M. Morikawa, M. Shimono, and C. Midorikawa for secretarial assistance. We are also grateful to staff members of the Proteomic Analysis Core-system on General Research Core Laboratory, Kumamoto University Medical School, for important contributions to the experiments.

* This work was supported by grants from Cancer Research (to N. A.), Kiban Research (to N. A.), and Houga Research (to N. A.) from the Ministry of Education, Culture, Sports, Science and Technology of Japan; from The Ministry of Health and Welfare of Japan (to N. A.); from the Japan Health Sciences Foundation (to D. K. and N. A.); and from the Center of Excellence project B of Kumamoto University for proteomics research and education (to N. A.).

[S] The on-line version of this article (available at http://www.mcponline.org) contains supplemental material.

‖ To whom correspondence should be addressed. Tel.: 81-96-373-5119; Fax: 81-96-373-5210; E-mail: nori@gpo.kumamoto-u.ac.jp.

REFERENCES

1. Ross, P. L., Huang, Y. N., Marchese, J. N., Williamson, B., Parker, K., Hattan, S., Khainovski, N., Pillai, S., Dey, S., Daniels, S., Purkayastha, S., Juhasz, P., Martin, S., Bartlet-Jones, M., He, F., Jacobson, A., and Pappin, D. J. (2004) Multiplexed protein quantitation in Saccharomyces cerevisiae using amine-reactive isobaric tagging reagents. *Mol. Cell. Proteomics* **3,** 1154–1169
2. Mann, M. (2006) Functional and quantitative proteomics using SILAC. *Nat. Rev. Mol. Cell Biol.* **7,** 952–958
3. Keller, M., Rüegg, A., Werner, S., and Beer, H. D. (2008) Active caspase-1 is a regulator of unconventional protein secretion. *Cell* **132,** 818–831
4. Wang, Z., Gucek, M., and Hart, G. W. (2008) Cross-talk between GlcNAcylation and phosphorylation: site-specific phosphorylation dynamics in response to globally elevated O-GlcNAc. *Proc. Natl. Acad. Sci. U.S.A.* **105,** 13793–13798
5. Graumann, J., Hubner, N. C., Kim, J. B., Ko, K., Moser, M., Kumar, C., Cox, J., Schöler, H., and Mann, M. (2008) Stable isotope labeling by amino acids in cell culture (SILAC) and proteome quantitation of mouse embryonic stem cells to a depth of 5,111 proteins. *Mol. Cell. Proteomics* **7,** 672–683
6. DeSouza, L. V., Grigull, J., Ghanny, S., Dubé, V., Romaschin, A. D., Colgan, T. J., and Siu, K. W. (2007) Endometrial carcinoma biomarker discovery and verification using differentially tagged clinical samples with multidimensional liquid chromatography and tandem mass spectrometry. *Mol. Cell. Proteomics* **6,** 1170–1182
7. Ralhan, R., Desouza, L. V., Matta, A., Chandra Tripathi, S., Ghanny, S., Datta Gupta, S., Bahadur, S., and Siu, K. W. (2008) Discovery and verification of head-and-neck cancer biomarkers by differential protein expression analysis using iTRAQ labeling, multidimensional liquid chromatography, and tandem mass spectrometry. *Mol. Cell. Proteomics* **7,** 1162–1173
8. Bantscheff, M., Eberhard, D., Abraham, Y., Bastuck, S., Boesche, M., Hobson, S., Mathieson, T., Perrin, J., Raida, M., Rau, C., Reader, V., Sweetman, G., Bauer, A., Bouwmeester, T., Hopf, C., Kruse, U., Neubauer, G., Ramsden, N., Rick, J., Kuster, B., and Drewes, G. (2007) Quantitative chemical proteomics reveals mechanisms of action of clinical ABL kinase inhibitors. *Nat. Biotechnol.* **25,** 1035–1044
9. Greene, L. A., and Tischler, A. S. (1976) Establishment of a noradrenergic clonal line of rat adrenal pheochromocytoma cells which respond to nerve growth factor. *Proc. Natl. Acad. Sci. U.S.A.* **73,** 2424–2428
10. Adler, E. M. (2006) Teaching resources. Cell culture as a model system for teaching: using PC12 cells. *Sci. STKE* **2006,** tr5
11. Yankner, B. A., Dawes, L. R., Fisher, S., Villa-Komaroff, L., Oster-Granite, M. L., and Neve, R. L. (1989) Neurotoxicity of a fragment of the amyloid precursor associated with Alzheimer's disease. *Science* **245,** 417–420
12. Apostol, B. L., Kazantsev, A., Raffioni, S., Illes, K., Pallos, J., Bodai, L., Slepko, N., Bear, J. E., Gertler, F. B., Hersch, S., Housman, D. E., Marsh,

J. L., and Thompson, L. M. (2003) A cell-based assay for aggregation inhibitors as therapeutics of polyglutamine-repeat disease and validation in Drosophila. *Proc. Natl. Acad. Sci. U.S.A.* **100,** 5950–5955
13. Ryu, E. J., Harding, H. P., Angelastro, J. M., Vitolo, O. V., Ron, D., and Greene, L. A. (2002) Endoplasmic reticulum stress and the unfolded protein response in cellular models of Parkinson's disease. *J. Neurosci.* **22,** 10690–10698
14. Yunoue, S., Tokuo, H., Fukunaga, K., Feng, L., Ozawa, T., Nishi, T., Kikuchi, A., Hattori, S., Kuratsu, J., Saya, H., and Araki, N. (2003) Neurofibromatosis type I tumor suppressor neurofibromin regulates neuronal differentiation via its GTPase-activating protein function toward Ras. *J. Biol. Chem.* **278,** 26958–26969
15. Feng, L., Yunoue, S., Tokuo, H., Ozawa, T., Zhang, D., Patrakitkomjorn, S., Ichimura, T., Saya, H., and Araki, N. (2004) PKA phosphorylation and 14-3-3 interaction regulate the function of neurofibromatosis type I tumor suppressor, neurofibromin. *FEBS Lett.* **557,** 275–282
16. Patrakitkomjorn, S., Kobayashi, D., Morikawa, T., Wilson, M. M., Tsubota, N., Irie, A., Ozawa, T., Aoki, M., Arimura, N., Kaibuchi, K., Saya, H., and Araki, N. (2008) Neurofibromatosis type 1 (NF1) tumor suppressor, neurofibromin, regulates the neuronal differentiation of PC12 cells via its associating protein, CRMP-2. *J. Biol. Chem.* **283,** 9399–9413
17. Davies, A. M. (1994) The role of neurotrophins in the developing nervous system. *J. Neurobiol.* **25,** 1334–1348
18. Chao, M. V. (2003) Neurotrophins and their receptors: a convergence point for many signalling pathways. *Nat. Rev. Neurosci.* **4,** 299–309
19. Lee, N. H., Weinstock, K. G., Kirkness, E. F., Earle-Hughes, J. A., Fuldner, R. A., Marmaros, S., Glodek, A., Gocayne, J. D., Adams, M. D., Kerlavage, A. R., Fraser, C. M., and Venter, J. C. (1995) Comparative expressed-sequence-tag analysis of differential gene expression profiles in PC-12 cells before and after nerve growth factor treatment. *Proc. Natl. Acad. Sci. U.S.A.* **92,** 8303–8307
20. Mayumi, K., Yaoi, T., Kawai, J., Kojima, S., Watanabe, S., and Suzuki, H. (1998) Improved restriction landmark cDNA scanning and its application to global analysis of genes regulated by nerve growth factor in PC12 cells. *Biochim. Biophys. Acta* **1399,** 10–18
21. Brown, A. J., Hutchings, C., Burke, J. F., and Mayne, L. V. (1999) Application of a rapid method (targeted display) for the identification of differentially expressed mRNAs following NGF-induced neuronal differentiation in PC12 cells. *Mol. Cell. Neurosci.* **13,** 119–130
22. Angelastro, J. M., Klimaschewski, L., Tang, S., Vitolo, O. V., Weissman, T. A., Donlin, L. T., Shelanski, M. L., and Greene, L. A. (2000) Identification of diverse nerve growth factor-regulated genes by serial analysis of gene expression (SAGE) profiling. *Proc. Natl. Acad. Sci. U.S.A.* **97,** 10424–10429
23. Dijkmans, T. F., van Hooijdonk, L. W., Schouten, T. G., Kamphorst, J. T., Vellinga, A. C., Meerman, J. H., Fitzsimons, C. P., de Kloet, E. R., and Vreugdenhil, E. (2008) Temporal and functional dynamics of the transcriptome during nerve growth factor-induced differentiation. *J. Neurochem.* **105,** 2388–2403
24. Garrels, J. I., and Schubert, D. (1979) Modulation of protein synthesis by nerve growth factor. *J. Biol. Chem.* **254,** 7978–7985
25. Sussman, M. A., Battenberg, E., Bloom, F. E., and Fowler, V. M. (1990) Identification of two nerve growth factor-induced polypeptides in PC12 cells. *J. Mol. Neurosci.* **2,** 163–174
26. Huang, C. M., Shui, H. A., Wu, Y. T., Chu, P. W., Lin, K. G., Kao, L. S., and Chen, S. T. (2001) Proteomic analysis of proteins in PC12 cells before and after treatment with nerve growth factor: increased levels of a 43-kDa chromogranin B-derived fragment during neuronal differentiation. *Brain Res. Mol. Brain Res.* **92,** 181–192
27. Huang, Y. H., Chang, A. Y., Huang, C. M., Huang, S. W., and Chan, S. H. (2002) Proteomic analysis of lipopolysaccharide-induced apoptosis in PC12 cells. *Proteomics* **2,** 1220–1228
28. Zhou, B., Yang, W., Ji, J. G., and Ru, B. G. (2004) Differential display proteome analysis of PC-12 cells transiently transfected with metallothionein-3 gene. *J. Proteome Res.* **3,** 126–131
29. Yang, W., Liu, P., Liu, Y., Wang, Q., Tong, Y., and Ji, J. (2006) Proteomic analysis of rat pheochromocytoma PC12 cells. *Proteomics* **6,** 2982–2990
30. Shilov, I. V., Seymour, S. L., Patel, A. A., Loboda, A., Tang, W. H., Keating, S. P., Hunter, C. L., Nuwaysir, L. M., and Schaeffer, D. A. (2007) The Paragon Algorithm, a next generation search engine that uses sequence temperature values and feature probabilities to identify peptides from tandem mass spectra. *Mol. Cell. Proteomics* **6,** 1638–1655
31. Carbon, S., Ireland, A., Mungall, C. J., Shu, S., Marshall, B., and Lewis, S. (2009) AmiGO: online access to ontology and annotation data. *Bioinformatics* **25,** 288–289
32. Kondili, K., Tsolas, O., and Papamarcaki, T. (1996) Selective interaction between parathymosin and histone H1. *Eur. J. Biochem.* **242,** 67–74
33. Ueda, H., Fujita, R., Yoshida, A., Matsunaga, H., and Ueda, M. (2007) Identification of prothymosin-alpha1, the necrosis-apoptosis switch molecule in cortical neuronal cultures. *J. Cell Biol.* **176,** 853–862
34. Heaton, J. H., Dlakic, W. M., Dlakic, M., and Gelehrter, T. D. (2001) Identification and cDNA cloning of a novel RNA-binding protein that interacts with the cyclic nucleotide-responsive sequence in the Type-1 plasminogen activator inhibitor mRNA. *J. Biol. Chem.* **276,** 3341–3347
35. Soeda, S., Shinomiya, K., Ochiai, T., Koyanagi, S., Toda, A., Eyanagi, R., and Shimeno, H. (2006) Plasminogen activator inhibitor-1 aids nerve growth factor-induced differentiation and survival of pheochromocytoma cells by activating both the extracellular signal-regulated kinase and c-Jun pathways. *Neuroscience* **141,** 101–108
36. Wang, D., and Gao, L. (2005) Proteomic analysis of neural differentiation of mouse embryonic stem cells. *Proteomics* **5,** 4414–4426
37. Rodríguez, P., Viñuela, J. E., Alvarez-Fernández, L., Buceta, M., Vidal, A., Domínguez, F., and Gómez-Márquez, J. (1998) Overexpression of prothymosin alpha accelerates proliferation and retards differentiation in HL-60 cells. *Biochem. J.* **331,** 753–761
38. Salehi, A. H., Roux, P. P., Kubu, C. J., Zeindler, C., Bhakar, A., Tannis, L. L., Verdi, J. M., and Barker, P. A. (2000) NRAGE, a novel MAGE protein, interacts with the p75 neurotrophin receptor and facilitates nerve growth factor-dependent apoptosis. *Neuron* **27,** 279–288
39. Stapels, M. D., and Barofsky, D. F. (2004) Complementary use of MALDI and ESI for the HPLC-MS/MS analysis of DNA-binding proteins. *Anal. Chem.* **76,** 5423–5430
40. Possenti, R., Eldridge, J. D., Paterson, B. M., Grasso, A., and Levi, A. (1989) A protein induced by NGF in PC12 cells is stored in secretory vesicles and released through the regulated pathway. *EMBO J.* **8,** 2217–2223
41. Mobarak, C. D., Anderson, K. D., Morin, M., Beckel-Mitchener, A., Rogers, S. L., Furneaux, H., King, P., and Perrone-Bizzozero, N. I. (2000) The RNA-binding protein HuD is required for GAP-43 mRNA stability, GAP-43 gene expression, and PKC-dependent neurite outgrowth in PC12 cells. *Mol. Biol. Cell* **11,** 3191–3203
42. Laslop, A., and Tschernitz, C. (1992) Effects of nerve growth factor on the biosynthesis of chromogranin A and B, secretogranin II and carboxypeptidase H in rat PC12 cells. *Neuroscience* **49,** 443–450
43. Jacovina, A. T., Zhong, F., Khazanova, E., Lev, E., Deora, A. B., and Hajjar, K. A. (2001) Neuritogenesis and the nerve growth factor-induced differentiation of PC-12 cells requires annexin II-mediated plasmin generation. *J. Biol. Chem.* **276,** 49350–49358
44. Aletta, J. M., Angeletti, R., Liem, R. K., Purcell, C., Shelanski, M. L., and Greene, L. A. (1988) Relationship between the nerve growth factor-regulated clone 73 gene product and the 58-kilodalton neuronal intermediate filament protein (peripherin). *J. Neurochem.* **51,** 1317–1320
45. Stroth, U., Meffert, S., Gallinat, S., and Unger, T. (1998) Angiotensin II and NGF differentially influence microtubule proteins in PC12W cells: role of the AT2 receptor. *Brain Res. Mol. Brain Res.* **53,** 187–195
46. Lorusso, A., Covino, C., Priori, G., Bachi, A., Meldolesi, J., and Chieregatti, E. (2006) Annexin2 coating the surface of enlargeosomes is needed for their regulated exocytosis. *EMBO J.* **25,** 5443–5456
47. Lawrence, D. A., Strandberg, L., Ericson, J., and Ny, T. (1990) Structure-function studies of the SERPIN plasminogen activator inhibitor type 1. Analysis of chimeric strained loop mutants. *J. Biol. Chem.* **265,** 20293–20301
48. Bommer, U. A., and Thiele, B. J. (2004) The translationally controlled tumour protein (TCTP). *Int. J. Biochem. Cell Biol.* **36,** 379–385
49. Yang, Y., Yang, F., Xiong, Z., Yan, Y., Wang, X., Nishino, M., Mirkovic, D., Nguyen, J., Wang, H., and Yang, X. F. (2005) An N-terminal region of translationally controlled tumor protein is required for its antiapoptotic activity. *Oncogene* **24,** 4778–4788
50. Baharvand, H., Fathi, A., Gourabi, H., Mollamohammadi, S., and Salekdeh, G. H. (2008) Identification of mouse embryonic stem cell-associated proteins. *J. Proteome Res.* **7,** 412–423
51. Segade, F., and Gómez-Márquez, J. (1999) Prothymosin alpha. *Int. J. Biochem. Cell Biol.* **31,** 1243–1248

52. Gómez-Márquez, J. (2007) Function of prothymosin alpha in chromatin decondensation and expression of thymosin beta-4 linked to angiogenesis and synaptic plasticity. *Ann. N.Y. Acad. Sci.* **1112,** 201–209
53. Barrett, G. L., Greferath, U., Barker, P. A., Trieu, J., and Bennie, A. (2005) Co-expression of the P75 neurotrophin receptor and neurotrophin receptor-interacting melanoma antigen homolog in the mature rat brain. *Neuroscience* **133,** 381–392
54. Xue, B., Wen, C., Shi, Y., Zhao, D., and Li, C. (2005) Human NRAGE disrupts E-cadherin/beta-catenin regulated homotypic cell-cell adhesion. *Biochem. Biophys. Res. Commun.* **336,** 247–251
55. Quinn, C. C., Chen, E., Kinjo, T. G., Kelly, G., Bell, A. W., Elliott, R. C., McPherson, P. S., and Hockfield, S. (2003) TUC-4b, a novel TUC family variant, regulates neurite outgrowth and associates with vesicles in the growth cone. *J. Neurosci.* **23,** 2815–2823

Cancer Science
The official journal of the Japanese Cancer Association JCA

Contribution of BCR–ABL-independent activation of ERK1/2 to acquired imatinib resistance in K562 chronic myeloid leukemia cells

Takeru Nambu,[1] Norie Araki,[2,5] Aiko Nakagawa,[1] Akihiko Kuniyasu,[3] Tatsuya Kawaguchi,[4] Akinobu Hamada[1] and Hideyuki Saito[1,5]

[1]Department of Pharmacy, Kumamoto University Hospital, Kumamoto; [2]Department of Tumor Genetics and Biology, Graduate School of Medical Sciences, Kumamoto University School of Medicine, Kumamoto; [3]Department of Molecular Cell Function, Graduate School of Pharmaceutical Sciences, Kumamoto University, Kumamoto; [4]Department of Hematology and Infectious Diseases, Kumamoto University Hospital, Kumamoto, Japan

(Received July 3, 2009/Revised September 4, 2009/Accepted September 8, 2009/Online publication October 14, 2009)

BCR–ABL tyrosine kinase, generated from the reciprocal chromosomal translocation t(9;22), causes chronic myeloid leukemia (CML). BCR–ABL is inhibited by imatinib; however, several mechanisms of imatinib resistance have been proposed that account for loss of imatinib efficacy in patients with CML. Previously, we showed that overexpression of the efflux drug transporter P-glycoprotein partially contributed to imatinib resistance in imatinib-resistant K562 CML cells having no BCR–ABL mutations. To explain an additional mechanism of drug resistance, we established a subclone (K562/R) of the cells and examined the BCR–ABL signaling pathway in these and wild-type K562 (K562/W) cells. We found the K562/R cells were 15 times more resistant to imatinib than their wild-type counterparts. In both cell lines, BCR–ABL and its downstream signaling molecules, such as ERK1/2, ERK5, STAT5, and AKT, were phosphorylated in the absence of imatinib. In both cell lines, imatinib effectively reduced the phosphorylation of all the above, except ERK1/2, whose phosphorylation was, interestingly, only inhibited in the wild-type cells. We then observed that phospho-ERK1/2 levels decreased in the presence of siRNA targeting BCR–ABL, again, only in the K562/W cells. However, using an ERK1/2 inhibitor, U0126, we found that we could reduce phospho-ERK1/2 levels in K562/R cells and restore their sensitivity to imatinib. Taken together, we conclude that the BCR–ABL-independent activation of ERK1/2 contributes to imatinib resistance in K562/R cells, and that ERK1/2 could be a target for the treatment of CML patients whose imatinib resistance is due to this mechanism. (*Cancer Sci* 2010; 101: 137–142)

Chronic myeloid leukemia, a hematopoietic stem cell disorder, is characterized by the expression of the chimeric BCR–ABL oncoprotein, caused by the reciprocal chromosomal translocation t(9;22) (q34;q11), which generates a shortened chromosome 22 or Philadelphia chromosome.[1] BCR–ABL is a cytoplasmic protein with constitutive tyrosine kinase activity responsible for transformation and leukemogenic effects. BCR–ABL is the target of the tyrosine kinase inhibitor imatinib, which also inhibits c-kit protooncogene/CD117 (c-KIT) and plate-derived growth factor receptor (PDGFR).[2] More than 90% of chronic-phase CML patients respond to imatinib, at least initially, and a high percentage of them achieve cytogenic complete responses.[3] However, some patients fail to respond to treatment with imatinib in front-line therapy (primary resistance), while others stop responding after an initial response (acquired resistance).[4] Frequent clinical relevancies to imatinib resistance include point mutations in the *ABL* gene[5,6] and amplification of the *BCR–ABL* fusion gene.[7] In addition to these BCR–ABL-dependent mechanisms, BCR–ABL-independent mechanisms of imatinib resistance have been proposed, which involve the drug transporter P-gp (MDR1, ATP-binding cassette subfamily B1 (ABCB1)),[8–10] the drug carrier serum α_1 acid glycoprotein,[11] and signal cascades via LYN kinase.[12,13] Although some mechanisms of imatinib resistance are understood, resistance to this drug is still an important challenge confronting the effective treatment of CML.

We previously focused on drug transporters and reported the potential contribution to imatinib resistance of P-gp, a multidrug efflux transporter, using K562 cells, which are known as a representative human CML cell line.[9] In a previous study, we established imatinib-resistant K562 (prevK562/R) cells, which had wild-type BCR–ABL and overexpressed P-gp. In prevK562/R cells, intracellular imatinib levels were 42% less than those in wild-type K562 (K562/W) cells. Intracellular imatinib accumulation was restored completely by CysA, a P-gp inhibitor; however, CysA did not completely overcome prevK562/R cell sensitivity to imatinib. Therefore, we assumed that another mechanism was also involved in imatinib resistance in K562 cells. To identify this unknown mechanism, we focused on signal transduction pathways that were downstream of BCR–ABL, and analyzed imatinib resistance factors, other than overexpression of P-gp, using a new imatinib-resistant subclone of K562 (K562/R) cells, which was cloned from prevK562/R cells.

BCR–ABL has multiple downstream survival pathways, including ERK1/2, ERK5, AKT, JAK/STAT, nuclear factor kappa beta (NF-κB), and BCL-x_L.[14–18] Phosphorylation of tyrosine 177 of BCR–ABL is necessary for binding of the adaptor growth factor receptor-bound protein (GRB2) to BCR–ABL, which involves the recruitment of son of sevenless (SOS), the nucleotidic exchange factor of RAS.[19] RAS activates both the RAF–MEK–ERK1/2 and PI3K–AKT pathways, which are engaged in cell survival and anti-apoptosis.[18,20] ERK5, like ERK1/2, is a member of the mitogen-activated protein kinase family, is modulated by BCR–ABL, and contributes to the survival of leukemia cells.[17,21] In the present study, we investigated the contributions of these downstream factors to imatinib resistance in K562/R cells.

Here, we demonstrate that BCR–ABL-independent activation of ERK1/2 may contribute to imatinib resistance in certain CML cell lines. This resistance can be overcome by co-treatment with the specific ERK1/2 inhibitor and imatinib, indicating that this co-treatment may be effective for imatinib-resistant CML patients.

Materials and Methods

Cell culture and cloning of imatinib-resistant K562 cells. K562/W cells were cultured in RPMI-1640 medium supplemented with

[5]To whom correspondence should be addressed.
E-mail: saitohide@fc.kuh.kumamoto-u.ac.jp; nori@gpo.kumamoto-u.ac.jp

doi: 10.1111/j.1349-7006.2009.01365.x

10% FBS under an atmosphere of 5% CO_2–95% air at 37°C. prevK562/R cells were established by exposing gradually increasing concentrations of imatinib (from 0.3 to 10 μM) from K562/W cells.[9] The new clonal cell line K562/R was established by limiting dilution from prevK562/R cells. K562/R cells were maintained under the same culture conditions in the presence of 1 μM imatinib.

mRNA isolation and cDNA synthesis. For mRNA extraction, MagNA Pure LC mRNA Isolation Kit II (Roche Diagnostics, Basel, Switzerland) was used as per the instruction manual. cDNA was synthesized by reverse transcription using the High-Capacity cDNA Archive Kit (Applied Biosystems, Foster City, CA, USA). Each prepared cellular cDNA was stored at –30°C.

Mutation analysis of the *BCR–ABL* kinase domain and *KRAS*. The kinase domain of *BCR–ABL* was amplified by PCR using each cellular cDNA.[9] For the primary PCR, we used the forward primer 5′-CCAGACTGTCCACAGCATTC-3′ and the reverse primer 5′-ATGGTCCAGAGGATCGCTCTCT-3′, and for the secondary PCR, the forward primer 5′-GGGAGGGTGTACC-ATTACAGG-3′ and the reverse primer, 5′-GCTGTGTAGG-TGTCCCCTGT-3′, or the forward primer 5′-CCACTTGGTGA-AGGTAGCTG-3′ and the reverse primer, 5′-CCTGCAGCAA-GGTAGTCACA-3′, were used. The analysis was carried out by DNA sequencing using an Applied Biosystems 3130 Genetic Analyzer. For the mutation analysis of *KRAS ORF*, the forward primer 5′-CGGGAGAGAGGCCTGCTG-3′ and the reverse primer 5′-CCACTTGTACTAGTATGCCT-3′ were used in PCR amplification. The sequence of the *KRAS* gene was analyzed by the Sigma-Aldrich DNA sequencing Service.

Cytotoxicity assay. The individual or combined cytotoxicities of imatinib and U0126 were determined by the Alamar Blue assay as described previously.[9,22] Absorbance in cells without drug treatment was 100%.

Western blot analysis. K562/W and K562/R cells were homogenized in a solution containing 7 M urea, 2 M thiourea, 4% CHAPS, protease inhibitor cocktail (P8430; Sigma-Aldrich, St Louis, MO, USA), 2 mM Na_3VO_4, 10 mM NaF, 1 μM okadaic acid, and 1 mM DTT, using Micropestle (Eppendorf, Westbury, NY, USA). Crude membrane fraction selection and Western blotting conditions were as described previously.[9] The following primary antibodies were used: LYN, phospho-STAT5 (Tyr^{694}), STAT5 (BD Transduction Laboratories, Lexington, KY, USA), β-actin (Sigma-Aldrich), 4G10, Na^+/K^+ ATPase α-1 (Upstate Biotechnology, Lake Placid, NY, USA), c-ABL (Santa Cruz Biotechnology, Santa Cruz, CA, USA), phospho-ERK1/2, ERK1/2, phospho-AKT (Thr^{308}), phospho-AKT (Ser^{473}), AKT, ERK5 (Cell Signaling Technology, Beverly, MA, USA), and P-gp (C219 monoclonal antibody; Signet Laboratories, Dedham, MA, USA).

Two-dimensional Western blotting. Samples were desalted using the 2-D Clean-Up kit (GE Healthcare, Amersham Place, UK) and resolved with sample buffer (7 M urea, 2 M thiourea, 4% CHAPS, 0.5% IPG Buffer pH 3–10, and Destreaking buffer). The first-dimensional isoelectric focusing (pH 3–10, 7 cm) was carried out using the Ettan IPGPhor Cup Loading Manifold electrophoresis system (GE Healthcare) as per manufacturer recommendations. After reduction and alkylation of disulfide bonds with 10 mg/mL DTT and 25 mg/mL iodoacetamide, respectively, the second-dimensional separation was carried out by 12% SDS-PAGE. The 2D gel was immunoblotted as indicated above.

Real-time RT-PCR analysis. To determine the expression levels of *hMDR1* and *hβ-ACTIN* in the cells, we carried out TaqMan quantitative real-time RT-PCR using the ABI PRISM 7900 sequence detection system (Applied Biosystems), using the manufacturer's standard protocol (*hMDR1*, Hs00184491_m1; *hβ-ACTIN*, 4310881E).

Analysis of intracellular imatinib accumulation. Cells (2×10^6) were incubated in 5 mL incubation buffer (150 mM NaCl, 3 mM KCl, 1 mM $CaCl_2$, 0.5 mM $MgCl_2$, 5 mM D-glucose, 5 mM HEPES, pH 7.4) containing 1 μM imatinib. The cell pellet was washed once in ice-cold PBS containing 1% BSA, and twice with ice-cold PBS. The cellular imatinib was then extracted by incubation with 300 μL of 50% methanol (HPLC mobile phase/methanol = 1/1) for 30 min. Quantification of imatinib was done using the HPLC (model LC-6A; Shimadzu, Kyoto, Japan) method described previously.[8] For the cellular protein quantitation, the pellet was solubilized with 200 μL of 1 N NaOH and analyzed by the Bradford method, using a Bio Rad Protein Assay kit (Bio Rad, Hercules, CA, USA) with BSA as a standard.

siRNA transfection. An siRNA specific for the b3a2 breakpoint of the *BCR–ABL* gene (5′-GCAGAGUUCAAAAGCC-CUUdTdT), and a control siRNA composed of the scrambled b3a2 sequence (5′-GCAGAGUUCUAAAGCGCUUdTdT),[23] were synthesized by Nippon EGT (Toyama, Japan). For electroporation of K562/W and K562/R cells, we used Micro-Porator MP-100 (AR Brown, Tokyo, Japan). Cells were washed twice with PBS, and mixed with 20 μM stock siRNA to a final concentration of 3, 4 or 8 pmol/μL. Subsequently 5×10^5 cells/10 μL of the cell suspension were electroporated using the following settings: pulse voltage = 1450 V, pulse width = 10 ms, and pulse number = three times. After electroporation, the cells were resuspended in RPMI-1640 medium and cultured in the incubator for 48 h under the same conditions as other cells.

Statistical analysis. Statistical significance was determined by Welch's *t*-test. $P < 0.05$ was considered statistically significant.

Results

Characterization of imatinib-resistant K562/R cells. We established a new K562/R clonal cell line, which indicated a 15-fold increase in the IC_{50} of imatinib over the parent K562/W cells (Fig. 1A), had no mutation in the BCR–ABL kinase domain (data not shown), and had neither overexpression nor overactivation of BCR–ABL or LYN kinase (Fig. 1B). Mutation analysis of *KRAS* showed no missense mutations[24,25] in either cell line, although one silent mutation (519T > C) was found in both cells (Supporting information Fig. S1), suggesting that *KRAS* mutation in K562/R cells is not a factor in imatinib resistance. Both levels of mRNA (300-fold, $P < 0.01$; Fig. 1C) and protein in the crude membrane fraction (Supporting information Fig. S2B) of MDR1 were found to be elevated in K562/R cells compared with K562/W cells (almost similar results were obtained in prevK562/R cells[9]), although intracellular accumulation levels of imatinib were similar (Fig. 1D). Moreover, CysA, a P-gp inhibitor, did not influence intracellular imatinib accumulation levels in either type of cell. These results suggest that the imatinib resistance of K562/R cells is not directly related to the cellular P-gp expression level or function.

Imatinib did not inhibit the phosphorylation of ERK1/2 in K562/R cells. To study the specific activation signals in K562/R cells, K562/W and K562/R cells were treated with imatinib for varying lengths of time, as shown in Figure 2(A), after which the phosphorylation of BCR–ABL and its downstream factors, AKT, ERK5, STAT5, and ERK1/2 was examined. The phosphorylation levels of BCR–ABL and STAT5 were similarly high in both cell lines, but those of AKT and ERK1/2 were higher in the K562/R cells. After the treatment with imatinib, the phosphorylation of BCR–ABL, AKT, and STAT5 was effectively inhibited in both cell lines (Fig. 2A). ERK5 expression, which is known to be regulated by BCR–ABL,[17] was not decreased by imatinib in either cell line (Fig. 2A). To analyze the phosphorylation status of ERK5 in both cell lines, we carried out 2D Western blotting using anti-ERK5 antibodies after a 24-h treatment

doi: 10.1111/j.1349-7006.2009.01365.x

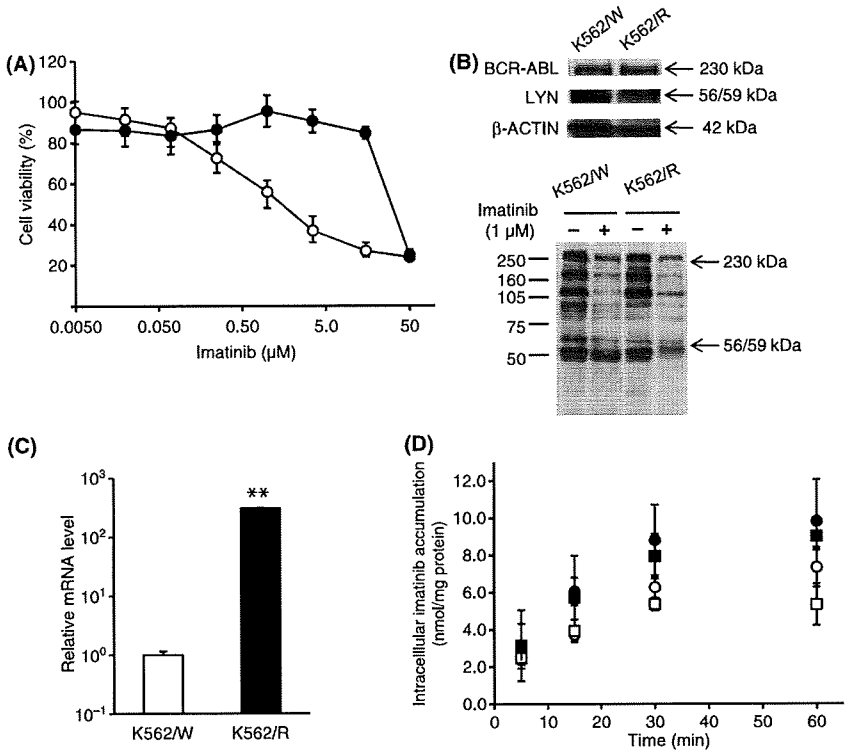

Fig. 1. Characteristics of imatinib-resistant K562/R cells. Imatinib and FBS were depleted from the medium 1 day before all experimental procedures to efflux intracellular imatinib from K562/R cells. (A) K562/W (open circles) and K562/R (closed circles) cells were exposed to various concentrations of imatinib for 48 h. Cell viability was assayed by Alamar Blue. Each point represents the mean ± SD from six cells. (B) The expression levels of BCR–ABL, LYN, and β-actin and phosphorylation of tyrosine were examined by Western blot analysis. K562/W and K562/R cells were treated with 1 μM imatinib for 15 min. (C) The mRNA levels of *hMDR1* and *hβ-ACTIN* were examined by real time RT-PCR analysis. The relative amount of *hMDR1* mRNA was normalized to that of *hβ-ACTIN*. (D) Intracellular imatinib accumulation was measured by HPLC analysis in K562/W and K562/R cells. The cells (2.0×10^6) were exposed to 1 μM imatinib with (squares) or without (circles) 5 μM cyclosporin A (CysA) at 37°C for varying lengths of time in K562/W (open symbols) and K562/R (closed symbols). Each point represents the mean ± SD from four cells. $^{**}P < 0.01$ *versus* K562/W cells.

with imatinib, and compared the 2D patterns of ERK5-positive spots (Fig. 2C). Prior to imatinib treatment, both cell lines showed at least two ERK5-positive spots in 2D Western blotting. After treatment, one of these spots, presumed to be phosphorylated ERK5, underwent a significant shift from left (acid, pI 4.7) to right (basic, pI 4.9), suggesting that the phosphorylation of ERK5 was inhibited by the imatinib treatment in both cell lines. In contrast, ERK1/2 phosphorylation was inhibited in K562/W cells only (Fig. 2A). Interestingly, imatinib inhibitory effects on the phosphorylation of BCR–ABL were significant in a dose-dependent manner, while phosphorylation of ERK1/2 was never downregulated by imatinib in K562/R cells (Fig. 2B). Results similar to the above were obtained in prevK562/R cells (Supporting information Fig. S2A) and eight other clones also established as imatinib-resistant K562 cells (Fig. 2D). These results strongly indicate that, unlike in K562/W cells, BCR–ABL does not play a major role in the phosphorylation of ERK1/2 in K562/R cells.

BCR–ABL-targeting siRNA decreased the phosphorylation of ERK1/2 in K562/W cells, but not in K562/R cells. To confirm that ERK1/2 was activated independently of BCR–ABL in K562/R cells, BCR–ABL-targeting siRNA was transfected into cells from both cell lines. Since K562 cells express the b3a2 form of the BCR–ABL fusion mRNA, the specific sequence for b3a2 can effectively silence cellular BCR–ABL expression.[23] Transient transfection with varying amounts of b3a2 BCR–ABL siRNA significantly reduced the expression of BCR–ABL protein but not that of c-ABL in K562/W cells, compared with cells transfected with a control scrambled siRNA (Fig. 3A). The same treatment also induced the downregulation of phosphorylated-ERK1/2 in K562/W cells; however, it did not have this effect on K562/R cells (Fig. 3B).

Inhibition of ERK1/2 overcame imatinib resistance in K562/R cells. Because the results obtained from the above experiments strongly suggested that the BCR–ABL-independent activation of ERK1/2 is directly related to the mechanism of imatinib resistance in K562/R cells, we examined the effect of ERK1/2 inhibition on these cells. Treatment with an ERK1/2 inhibitor, U0126,[26] alone for 48 h showed similar dose-dependent toxicity for K562/W and K562/R cells (Fig. 4A). Treatment with U0126 (1 μM) alone had little cytotoxic effect on either cells; however, in combination with imatinib, cell death increased dramatically, with both cells showing a similar sensitivity to imatinib (Fig. 4B). These results suggest that co-administration of the ERK1/2 inhibitor with imatinib could overcome imatinib resistance in K562/R cells.

Co-treatment of imatinib and U0126 inhibited phosphorylation of ERK1/2 in both K562/W and K562/R cells. Because co-administration of imatinib with U0126 restored imatinib sensitivity in K562/R cells, we next analyzed the inhibitory effect of imatinib on ERK1/2 phosphorylation by Western blotting in both cell lines exposed to U0126 alone or combined with imatinib. After U0126 treatment for 24 h, a dose-dependent downregulation of ERK1/2 phosphorylation in both cell lines was observed (Fig. 5). Interestingly, co-administration of 1 μM imatinib with 1 μM U0126 remarkably inhibited the phosphorylation of ERK1/2 in K562/R cells. These results confirm that the BCR–ABL-independent ERK1/2 activation is essential for imatinib resistance in K562/R cells.

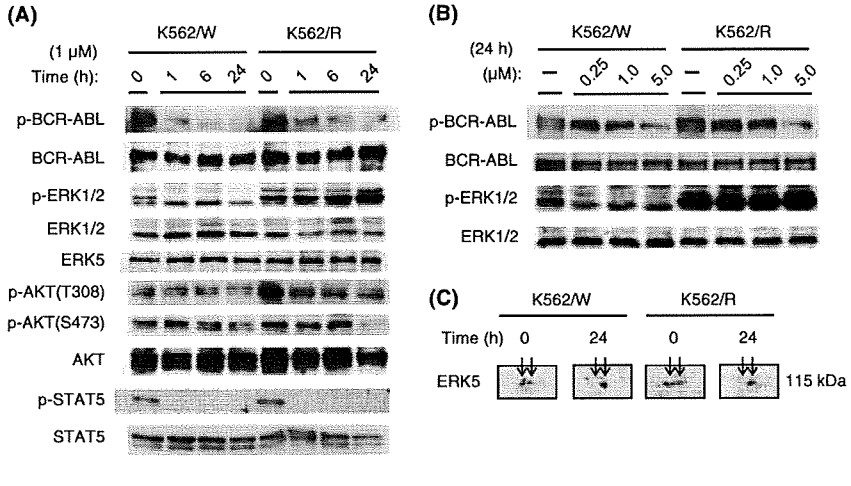

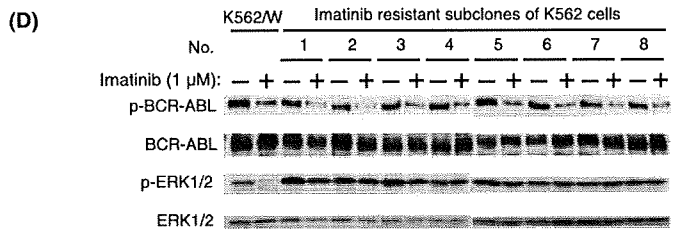

Fig. 2. Effects of imatinib on K562/W and K562/R cells were analyzed by immunoblotting. (A) Time course of BCR–ABL, ERK1/2, AKT, and STAT5 phosphorylation levels in K562/W and K562/R cells after 1 μM imatinib treatment. (B) Effect of the indicated concentrations of imatinib treatment for 24 h on the phosphorylation levels of BCR–ABL and ERK1/2 in K562/W and K562/R cells. (C) K562/W and K562/R cells were treated with 1 μM imatinib for 24 h. ERK5 was detected by 2D Western blotting. (D) K562/W and subcloned, imatinib-resistant K562 cells (from 1 to 8) were treated with 1 μM imatinib for 15 min. Clone cells of no. 2 is K562/R cells.

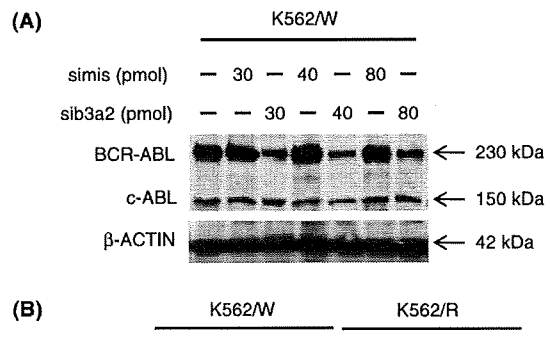

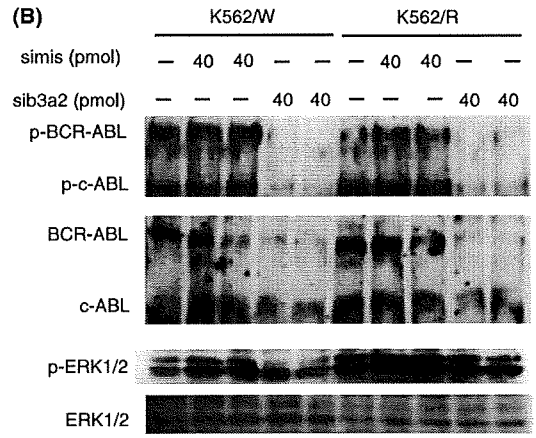

Fig. 3. Effects of BCR–ABL targeting siRNA on K562/W and K562/R cells. (A) K562/W cells were electroporated with different amounts of siRNA ranging from 30 to 80 pmol per 5×10^5 cells. (B) Effect of 40 pmol siRNA on the phosphorylation levels of BCR–ABL and ERK1/2 in K562/W and K562/R cells. sib3a2 and simis indicate BCR-ABL-specific siRNA and mismatch control siRNA, respectively.

Discussion

Despite the significant efficacy of imatinib in treating CML, the development of primary and acquired imatinib resistance is a problem in patients with CML. We previously reported that, although P-gp partly contributes to imatinib resistance in prevK562/R cells, P-gp function alone cannot fully explain the resistance to imatinib. We thus postulated the involvement of a separate mechanism, and established a new imatinib-resistant K562 clonal cell line (K562/R) from prevK562/R cells for use in studying this mechanism. In the new clonal cells, BCR–ABL was inhibited by both imatinib and BCR–ABL siRNA, while neither treatment suppressed ERK1/2 phosphorylation. Co-treatment with imatinib and the ERK1/2 inhibitor U0126 restored imatinib sensitivity in K562/R cells. These data suggested for the first time that ERK1/2, activated through a BCR–ABL-independent pathway, contributes to imatinib resistance in K562 cells.

Imatinib resistance is most often caused by BCR–ABL-dependent mechanisms, including point mutations in the functional kinase domain of BCR–ABL[5,6] and amplification of the *BCR–ABL* fusion gene.[7] Point mutations in *BCR–ABL* reduce the binding of imatinib to the protein by either a direct or an indirect mechanism. However, in our study, the K562/R cells showed neither *BCR–ABL* mutations nor overexpression (Fig. 1B), indicating that their imatinib resistance mechanism could involve a BCR–ABL-independent pathway. Similar mechanisms have been reported, namely, the overexpression of P-gp and LYN kinase.[10–13] Constitutively active mutants of KRAS are also known to be related to drug resistance in several cancers, including CML.[24,25,27–29] For example, mutations in *KRAS* codon 12 involving a substitution of valine for glycine or aspartic acid are known; however, these were not observed in our K562/W or K562/R cells. Although both cell lines had the 519T > C silent mutation at the translated region (Supporting information Fig. S1), this particular mutation would not seem to influence the sensitivity to imatinib. In addition, LYN, which is a member of the Src tyrosine kinase family and is reported to be involved in imatinib resistance through overexpression of the anti-apoptotic protein BCL-2,[12,13] is neither overexpressed nor overactivated in K562/R cells (Fig. 1B).

It is well known that imatinib interacts with P-gp as a substrate, and that overexpressed P-gp inhibits intracellular accumulation of imatinib.[8–10] In our study, although MDR1 mRNA and protein expression were higher in K562/R than K562/W

doi: 10.1111/j.1349-7006.2009.01365.x